

6333

AFCRL-62-1131

402803

CATALOGED BY ASTIA

AS AD NO. _____

402803

RESEARCH ON AEROSOL SCATTERING IN THE INFRARED

Scientific Report 10
Atlas of Scattering Diagrams for $n = 1.5$

Prepared by

Rudolf B. Penndorf

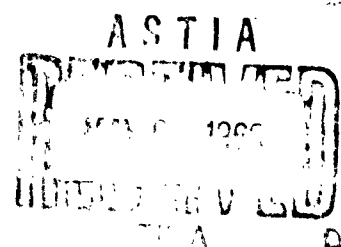
RESEARCH AND ADVANCED DEVELOPMENT DIVISION
AVCO CORPORATION
Wilmington, Massachusetts

Technical Report

RAD-TR-63-9

Contract AF19(604)-5743

November 1962



Prepared for

GEOPHYSICS RESEARCH DIRECTORATE
AIR FORCE CAMBRIDGE RESEARCH LABORATORIES
OFFICE OF AEROSPACE RESEARCH
UNITED STATES AIR FORCE
Bedford, Massachusetts

AFCRL-62-1131

This document consists of 60 pages,
259 copies, Series A

RESEARCH ON AEROSOL SCATTERING IN THE INFRARED

Scientific Report 10
Atlas of Scattering Diagrams for $n = 1.5$

Prepared by

Rudolf B. Penndorf

RESEARCH AND ADVANCED DEVELOPMENT DIVISION
AVCO CORPORATION
Wilmington, Massachusetts

Technical Report

RAD-TR-63-9

Contract AF19(604)-5743

November 1962

APPROVED


S. C. Coroniti, Manager
Space Science Department

Prepared for

GEOPHYSICS RESEARCH DIRECTORATE
AIR FORCE CAMBRIDGE RESEARCH LABORATORIES
OFFICE OF AEROSPACE RESEARCH
UNITED STATES AIR FORCE
Bedford, Massachusetts

NOTICE

Requests for additional copies by agencies of the Department of Defense, their contractors, and other Government agencies should be directed to:

ARMED SERVICES TECHNICAL INFORMATION AGENCY
ARLINGTON HALL STATION
ARLINGTON 12, VIRGINIA.

Department of Defense contractors must be established for ASTIA services or have their "need-to-know" certified by the cognizant military agency of their project or contract.

All other persons and organizations should apply to:

U. S. DEPARTMENT OF COMMERCE
OFFICE OF TECHNICAL SERVICES
WASHINGTON 25, D. C.

ABSTRACT

Angular scattering diagrams are constructed for spherical aerosols of refractive index $n = 1.5$. They show the intensity functions i_1 , i_2 , and $i_1 + i_2$ as functions of the scattering angles for size parameters $\alpha = 0.5 (0.5) 10$. The basic data have been computed using Mie's theory, and a graphical interpolation technique (altitude-chart technique) has been used to determine accurately the position and numerical value of the maxima and minima.

The scattering diagrams presented in this atlas allow to determine the intensity functions i_1 , i_2 , and $i_1 + i_2$ for any desired scattering angle with a high degree of reliability. The basic data limit the construction of reliable scattering diagrams to $\alpha < 10$.

ACKNOWLEDGMENT

The author gratefully acknowledges the assistance of Mr. F. Walsh who has carried out some of the computations and also prepared the illustrations.

CONTENTS

I.	Introduction	1
II.	Data	2
III.	Results	3
	3.1 Altitude Chart for Intensity Function i_1	3
	3.2 Altitude Chart for Intensity Function i_2	6
	3.3 Position of Dark Rings	7
	3.4 Diffraction Minima	7
	3.5 Scattering Diagrams	8
IV.	Conclusions	19
V.	Bibliography	20
VI.	Appendixes	21
	6.1 Atlas	21
	6.2 Table of Dark-Ring Parameters i_1 and i_2 , $n = 1.5$ and $\alpha = 0.5 (0.5) 10$	43

ILLUSTRATIONS

Figure	3-1	Altitude Chart for Intensity Function i_1 and $n = 1.5$ ($\rho < 10$)	9
	3-2	Altitude Chart for Intensity Function i_1 and $n = 1.5$ ($20 < \rho < 40$)	10
	3-3a	Position of Dark Rings and Center of Trenches in Altitude Chart for Intensity Function i_1 and $n = 1.5$	11
	3-3b	Diffraction and Reflection Minima for i_1 and $n = 1.5$	12
	3-4	Altitude Chart for Intensity Function i_2 and $n = 1.5$ ($\rho < 10$)	13
	3-5a	Position of Dark Rings and Center of Trenches in Altitude Chart for Intensity Function i_2 and $n = 1.5$	14
	3-5b	Diffraction and Reflection Minima for i_2 and $n = 1.5$	15
	3-6	Angular Position of Dark Rings for Intensity Function i_1 as Function of Size Parameter α for $n = 1.5$	16
	3-7	Angular Position of Dark Rings for Intensity Function i_2 as Function of Size Parameter α for $n = 1.5$	17
	3-8	Relative Intensity Function i_{1r} for the First Diffraction Minimum as Function of Diffraction Parameter u for $n = 1.5$	18

TABLES

Table	3-1	Position of Trenches for First Diffraction Minimum	4
	6-1	Data for Intensity Function i_1 and $D1$	44
	6-2	Data for Intensity Function i_1 , Diffraction	45
	6-3	Data for Intensity Function, Reflection System	46

I. INTRODUCTION

Theoretical data for angular scattering functions for spherical aerosols are needed for refractive indices n between 1.0 and 2.0. For $n = 1.33$, scattering diagrams have been published in an earlier report (Penndorf, 1961b). Herein, samples are given in the form of an atlas for $n = 1.5$, so that the user can take the needed information, from the curves, which is more reliable than a numerical interpolation of tabulated values. The interpolation technique is the same as in the last report. It had occurred to us that the samples given in steps of $\Delta\alpha = 0.5$ may not be sufficient; hence, a large number of workers in this field have been asked as to their preference of the steps to be selected. It turns out that for most practical application an atlas in steps of $\Delta\alpha = 0.5$ seems to be sufficient; however, for more detailed evaluations, the original tables are desirable. It is planned to publish these in the future also.

Computations of scattering functions for isotropic spherical nonabsorbing aerosols are based on Mie's theory, which leads to exact numerical values. The basic quantities are the intensity function i_1 and i_2 . They have the following meaning: the intensity function i_1 and i_2 are proportional to the magnitude of the two incoherent, plane-polarized components scattered by one particle; i_1 is proportional to the intensity whose electric oscillations are perpendicular to the plane of scattering; i. e., polarized light in the horizontal plane; i_2 is proportional to the intensity whose electric oscillations are in the plane of scattering; i. e., polarized light in the vertical plane.

The number of diagrams in the atlas is limited to the range $\alpha = 0.5$ to 10.0, because the reliability for interpolation decreases above $\alpha = 10$, as has been discussed in the last report, so that it does not seem justified to construct diagrams for large α values although numerical data exist up to $\alpha = 30$ for scattering angles 1 (1) 10 (10) 180° (Penndorf-Goldberg, 1953).

II. DATA

The atlas is based on numerical values for the intensity functions i_1 and i_2 which have been computed using an IBM 701 (Penndorf-Goldberg, 1953). They are available for a refractive index $n = 1.5$, size parameters $\alpha = 0.1$ (0.1) 30, and scattering angles $\theta = 0$ (1) 10 (10) 180°, where $\theta = 0^\circ$ defines the scattering angle in the forward direction.

A detailed table containing i_1 and i_2 in the same steps of $\Delta\theta$ but for $\alpha = 0.2$ (0.2) 159 has been published by Giese et al (1962) and used for comparison and detail above $\alpha = 30$ in the range $\theta = 0$ to 10° . The listed values for i_1 and i_2 agree very well with our table. In addition, Olaf and Robock (1961) and Robock (1962) have published scattering diagrams for $n = 1.5$ and $\alpha = 2, 8, 10, 20, 26,$ and 30 . Their basic computations have been quite detailed; namely, steps of $\Delta\theta = 2^\circ$ for $\alpha < 10$ and $\Delta\theta = 1^\circ$ for $\alpha > 12$. The scattering diagram for $\alpha = 8$ has been found useful, that for $\alpha = 10$ is very difficult to read and could be used only partially.

The investigation of our data shows that the steps of $\Delta\alpha = 0.1$ in the size parameter are sufficient, but the choice of scattering angles; namely, a constant step of $\Delta\theta = 10^\circ$, was unfortunate. While this step is sufficient to describe the intensity functions up to about $\alpha = 3$, it is in general insufficient for larger values of α as far as simple numerical interpolation is concerned. Only with the help of sophisticated graphical interpolation techniques is it possible to extend the useful limit of the tabulated values to about $\alpha = 10$. It is not recommended to interpolate our tables for $\alpha > 10$ except for the first diffraction minimum.

III. RESULTS

3.1 ALTITUDE CHART FOR INTENSITY FUNCTION i_1

The interpolation methods have been discussed in detail in the last report. Hence, there seems to be no need for repeating them. The altitude charts have been constructed for i_1 and i_2 , and the basic features appear similar to those for $n = 1.33$. The altitude chart for i_1 for the range of $\alpha < 10$ is shown in figure 3-1, for the range $20 < \alpha < 40$ in figure 3-2. For the range $10 < \alpha < 40$, an altitude chart for $0^\circ < \theta < 10^\circ$ has been plotted.

Two completely different types of contours appear on figure 3-1, one for $\theta < 90^\circ$ and another for $90 < \theta < 180^\circ$. In the forward scattering area, large, wide, and flat ridges are found, the peaks of which (indicated by the letter H) occur at larger ρ values* the larger u . For $u = 0$, a peak occurs at $\rho = 6$; for $u = 3.6$, at $\rho = 6.5$ and 7.5 ; and for $u = 6.0$, at $\rho = 8.8$; while the fourth peak is situated outside of this chart. The peaks are situated on ridges, which are cut off by quasi-vertical running valleys into which deep trenches are embedded. The valleys show some meandering around the classical diffraction values; namely, $u = 3.83, 7.02, \text{ and } 10.17$, which they approach asymptotically for very large values of ρ . Deep trenches occur systematically in each valley. Investigating the first diffraction minimum up to $\alpha = 40$ (figures 3-1 and 3-2), which can be done because data for i_1 and i_2 are available in steps of $\Delta\theta = 1^\circ$ up to $\theta = 10^\circ$, it was found that these trenches occur at $\rho = 7.2, 10.6, 19.6, 23.4, 26.3, 29.8, 32.2, 36.1, \text{ and } 38.8$. The range $10 < \alpha < 18$ is difficult to evaluate, and the trench position is not very accurate. Therefore, we have not estimated any values in this range now but will do so as the next step. Hence, the trenches are formed at intervals of $\Delta\rho \approx \pi$, whenever u reaches an extreme value (maximum or minimum). This again is an important result because the position of the deepest points of the trenches can be estimated without additional computations.

The position of the trenches has been investigated further. For $\rho > 6$, the first diffraction minimum occurs at scattering angles $\theta < 20^\circ$. The cross section theorem relates the total scattering coefficient K and $i_1 \left\{ 0 \right\}$. Hence, the question arises whether a useful relationship exists between K and $i_1 \left\{ 1^{\text{st}} \text{ min} \right\}$. It turns out that K reaches a maximum or minimum at the same size parameter ρ at which the deepest point occurs in the trenches of the first diffraction minimum. This particular ρ value is independent of n in the range $1.0 < n < 1.5$. It has not been checked for larger n values, but it is believed that this rule is valid up to about $n = 2$.

* ρ is the normalized size parameter and defined as $\rho = 2\alpha(n - 1)$. In the case of $n = 1.5$, $\rho \equiv \alpha$. The diffraction parameter is defined in the last report.

The results are shown in table 3-1. The running integer y indicates the first, second... trench. The first group shows the trench position related to $u < 3.83$ when K reaches a minimum, the second group contains those where $u > 3.83$ and K reaches a maximum. The position for K when $n \approx 1.0$ is given in the first column (after Penndorf, 1958), the second column the trench position for $n = 1.33$ (Penndorf, 1961a), and the last column for $n = 1.5$ as obtained from figures 3-1 and 3-2 and unpublished parts of our altitude charts. It is seen that the position of the trench is systematic and can be expressed as

$$\rho_T = 2\pi(y \pm 1/4),$$

where ρ_T is the position of a trench (or a maximum and minimum in K). The plus sign refers to $u < 3.83$ and a minimum in K ; the minus sign refers to $u > 3.83$ and a maximum in K . Interpolated values are shown in parentheses (). In the case when K reaches a maximum, the agreement is very good; in the case of K reaching a minimum, the trench occurs a bit earlier ($\Delta\rho \approx 0.3 - 0.5$). The agreement for $y = 1$ is always poor, as expected.

TABLE 3-1

POSITION OF TRENCHES FOR FIRST DIFFRACTION MINIMUM

y	K_{\min} and $u < 3.83$			K_{\max} and $u > 3.83$		
	K n = 1.0	i_1 1.33	i_1 1.5	K n = 1.0	i_1 1.33	i_1 1.5
1	7.6	6.9	7.2	4.1	---	---
2	14.0	13.5	(13.5)	10.8	9.9	10.6
3	20.3	19.8	19.6	17.2	16.8	(17.0)
4	26.6		26.3	23.5		23.4
5	32.9		32.2	29.8		29.8
6	39.2		38.8	36.1		36.1
	$\rho_T = 2\pi(y + 1/4)$			$\rho_T = 2\pi(y - 1/4)$		

The table lists the value ρ at which the maxima and minima in K occur for $u = 1.0$ and the deepest point of trenches for i_1 and $n = 1.33$ as well as $n = 1.5$.

For the second diffraction minimum, the first trench is found at $\rho = 6.5$ and $u = 5.5$, and the next at $\rho = 9.0$. Because of the interval $\Delta\theta = 10^\circ$ in this domain of the altitude chart, the last one cannot be exactly located.

Other diffraction minima have also been identified and can be seen on the chart. Basically, the system is similar to that of $n = 1.33$ and the minima start between $\theta = 80$ and 90° and move toward smaller angles as ρ increases.

However, there are differences in the charts for $n = 1.33$ and 1.50 , which are based on a more careful investigation for $n = 1.40, 1.44,$ and 1.50 , and which have led to several improvements. One point is the merging of diffraction minima. Whenever the first diffraction reaches a trench where u is a maximum, the first and second diffraction minima merge. This is seen on figure 3-1 at $u = 4.6$ and $\rho = 9.5$, and even better on figure 3-2. In the area $\rho > 23$, both diffraction minima come close together and run parallel for a while. The two valleys are definitely separated by a ridge of higher values with a peak around $\rho = 24.6$. It is drawn as if the first minimum ends near $\rho = 25.5$, but it could have been continued and both connected at $\rho = 26.3$. From a practical point of view, it is unimportant whether they actually merge or run parallel for a while. The distance between the two minima is about 1° for $\rho = 20$ to 30 and could not be distinguished on a scattering diagram. The same thing happens again around $\rho = 29.8$, where both minima run parallel for a while finally to merge at about $\rho = 31.4$. From this detailed study, based on figure 3-2, it is concluded that the actual merger of minima takes place and our interpretation at $\rho = 9.5$ is probably correct. The consequence of such mergers is a gradual reduction of the number of minima indicating the incorrectness of our earlier extrapolation (table I, Penndorf, 1961b). Rowell (private communication) has completed studies for $n = 1.486$ in steps of 1° and his interpretation does not show mergers as we have discussed them, but a termination of the first minimum whenever it reaches its lowest value of u . It seems important to us to check this point further and clarify the interpretation of the data to see whether our interpretation or that of Rowell is correct.

The backscatter area ($\theta > 90^\circ$) shows an entirely different pattern of the contours. Deep, long valleys occur in nearly straight lines into which deep trenches are embedded at regular intervals. The valleys meander somewhat around a straight line, but much less than the diffraction minima. The position and depth of the valleys are more difficult to establish than for $n = 1.33$, because the selected spacing of $\Delta\theta = 10^\circ$ is too wide for large α . However, basically, the interpolation problem up to $\alpha = 10$ is not too difficult. The distance between the centers of the trenches for a particular valley is about $\Delta\rho \approx 0.8$. This value is somewhat larger than for $n = 1.33$, where it was found to be about 0.65 to 0.75 .

For $\rho = 8.0$, our data can be compared with the scattering diagram published by Olaf and Robock (1961), and it is believed that they agree more or less with our evaluation (figure 3-1 and the appendixes). However, the curve for $\alpha = 10.0$ published by Robock (1962) is difficult to evaluate and could not be used.

The minima shown in figure 3-1 are redrawn on figure 3-3a, where the dots indicate the position of the trenches. It seems possible to us to explain the position of trenches as well as the system of the minima (dark rings). In our last report, we have already indicated a plausible interpretation of the position of the dark rings for i_2 and $n = 1.33$ as a combination of diffraction minima and reflection minima. This line of investigation is now pursued further. The term reflected ray is used for those rays which hit the spherical particles and undergo internal reflections and refractions at the surface (see figure 37 in van de Hulst, p. 201 (1957)).

A very detailed and careful analysis of the original data in the altitude chart (figure 3-1 only shows selected isolines) leads to two systems, which are indicated on figure 3-3b. The solid line system (diffraction minima) always starts at $\theta = 180^\circ$, it moves toward the 90° area more or less at a constant ρ value, and then with a sharp knee downward. The second system of dashed lines (reflection minima) runs more or less parallel to the $\theta = 180^\circ$ line. These two systems intersect each other at the trenches (dots on figure 3-3b, which are identical with those on figure 3-3a). We interpret this finding in the following way. The solid lines represent the minima caused by diffraction and the dashed lines those by internal reflection and refraction. Whenever these two systems cross each other, a trench is created. This seems plausible because the trenches are then caused by interference.

We have in the past, and also in figure 3-1, tried to follow the deepest minimum and, therefore, found some strange movements of the dark rings and sometimes extreme difficulties in deciding how to connect the minima. The suggested interference of the two systems explains our difficulties. It shows that sometimes the diffraction effect is a bit larger than the reflection effect, and the overall effect follows the solid lines in figure 3-2; at other times, the reverse is true. In addition, the interference can also lead to very weak minima when both systems arrive at opposite phase but equal amplitude. Furthermore, the meandering of the minima in the backward area can be explained as the interference of the two systems leading to a deviation from the straight reflection system. If, however, the minima follow a straight line with no meandering, then one system predominates and the other system contributes very little.

If another type of altitude chart were used in which the angles 90° to 180° were distributed according to another formula than the presently used one, such that $\theta = 180^\circ$ were plotted along the abscissa for $\rho = 0$, then the diffraction minima in the backward area would follow a vertical straight line similar to the forward area. Such a different altitude chart might be useful and should be explored to simplify the interpretation.

3.2 ALTITUDE CHART FOR INTENSITY FUNCTION i_2

The pattern on this altitude chart is generally similar to that for i_1 although less contour lines appear (figure 3-4). Hence, most of the statements and conclusions

made for i_1 apply. The description given for $n = 1.33$ is also valid and need not be repeated. Here again, figure 3-5a shows the minima taken from figure 3-4, and figure 3-5b contains the two intersecting systems. A comparison of figures 3-5a and 3-5b reveals the interaction of the two systems as discussed in section 3.2 for i_1 .

3.3 POSITION OF DARK RINGS

Based on the altitude charts, new graphs for the position of the dark rings have been constructed and are shown in figures 3-6 and 3-7 up to $\alpha = 10$. These figures supersede the curves given in an earlier report (Penndorf, 1961b) and are basically similar to those for $n = 1.33$. The dashed line indicates inflection points only and no real minima. In addition, the two systems described in section 3.1 are added. The system for diffraction minima is indicated by thin dashed lines going from the lower right-hand side to the upper left-hand side, and the system for reflection minima by thin dotted lines going more or less perpendicular to the first system. In general, the actual minima follow one or the other system. Meandering indicates that both systems are of about equal magnitude. In these cases, our interpretation of the continuous, predominant minimum may not always be correct, and a more detailed investigation based on data available in smaller steps than $\Delta\theta = 10^\circ$ may change our interpretation, especially around $\theta = 90^\circ$. Hence, we are convinced that the dividing zone between forward and backward movement is not of great importance and not fixed. Thus, it is believed that our earlier interpretation that the dividing zone is situated around $\theta = 80^\circ$ to 90° is erroneous. Data analysis for other refractive indices; for example, $n = 1.10, 1.20, 1.40,$ and $1.44,$ support our present viewpoint.

Rowell (private communication) has completed similar studies for $n = 1.486$ and finds a much more complicated pattern, such that nearly all of his dark rings move to larger scattering angles with increasing size parameter. Hence, the question of the true pattern is not yet solved. Only computations in smaller steps of θ can prove or disprove our interpretation.

3.4 DIFFRACTION MINIMA

A careful investigation of the diffraction minima can also lead to an improvement of the scattering diagrams because the angular position and the depths for a particular diffraction minimum changes systematically as seen on the altitude charts. The depth of the valley for a particular α value is defined by

$$i_{1r} \{ Dl, \alpha \} = \frac{i_1 \{ Dl, \alpha \}}{i_1 \{ 0^\circ, \alpha \}} ;$$

namely, the ratio of i_1 at the lowest point of the valley for a given θ value to the value i_1 in the forward direction ($\theta = 0^\circ$). The parameter D1 means first diffraction minimum. An analog definition applies to the higher orders of diffraction minima (D2, D3, and so on) as well as for i_2 .

Data of such i_{1r} and i_{2r} have been computed for all diffraction minima and plotted in a coordinate system, using u as abscissa and $\log i_{1r}$ as ordinate. For the first diffraction minimum, data up to $\alpha = 40$ are available; for the rest, only up to $\alpha = 10$. Since all diagrams are similar, only that for D1 is shown as an example in figure 3-8 because it is the most complete one. The data for $\alpha = 10$ to $\alpha = 19$ are less certain than the rest because $\Delta\theta > 10^\circ$ in this size range. Therefore, they are left out, also the data from $\alpha = 2$ to $\alpha = 5.5$ are omitted because, for such small α values, the pure diffraction pattern is not yet established.

From $\alpha = 5.5$ to 6.5 , a counterclockwise motion begins followed by a clockwise motion to $\alpha = 9.5$. The next curve begins at $\alpha = 19$ in a counterclockwise motion to 19.6 , is followed by a clockwise motion to $\alpha = 23.4$, and so forth. The minima for $u > 3.83$ are lower than those for $u < 3.83$. The lowest values of i_{1r} (the trenches on the altitude chart) occur always when u reaches a maximum or minimum for the counterclockwise motion. This simple system of clockwise and counterclockwise motion has been proven first for $n = 1.33$ and can be established now also for $n = 1.5$ and to higher values of ρ . It has been suggested in the report for $n = 1.33$ that the relation given in section 3.1 exists, and this is now proven. For all n 's, the minima of i_{1r} follow the relation

$$\rho_T = 2\pi(y \pm 1/4)$$

except for $y = 1$, and some slight deviation from this expression may be real. For the other diffraction minima, the same relation should hold, but more data in smaller steps of θ are needed to prove it.

3.5 SCATTERING DIAGRAMS

To visualize the numerical results and to show the correct interpolation of the tabulated data, a graphical presentation of the intensity functions i_1 , i_2 , and $i_1 + i_2$ has been prepared in the form of scattering diagrams for $\alpha = 0$ to 10 steps of $\Delta\alpha = 0.5$; they are given in appendix 6.1. The logarithmic scale chosen was such to allow reasonable interpolation.

The method of construction is the same as for $n = 1.33$ and, therefore, not repeated.

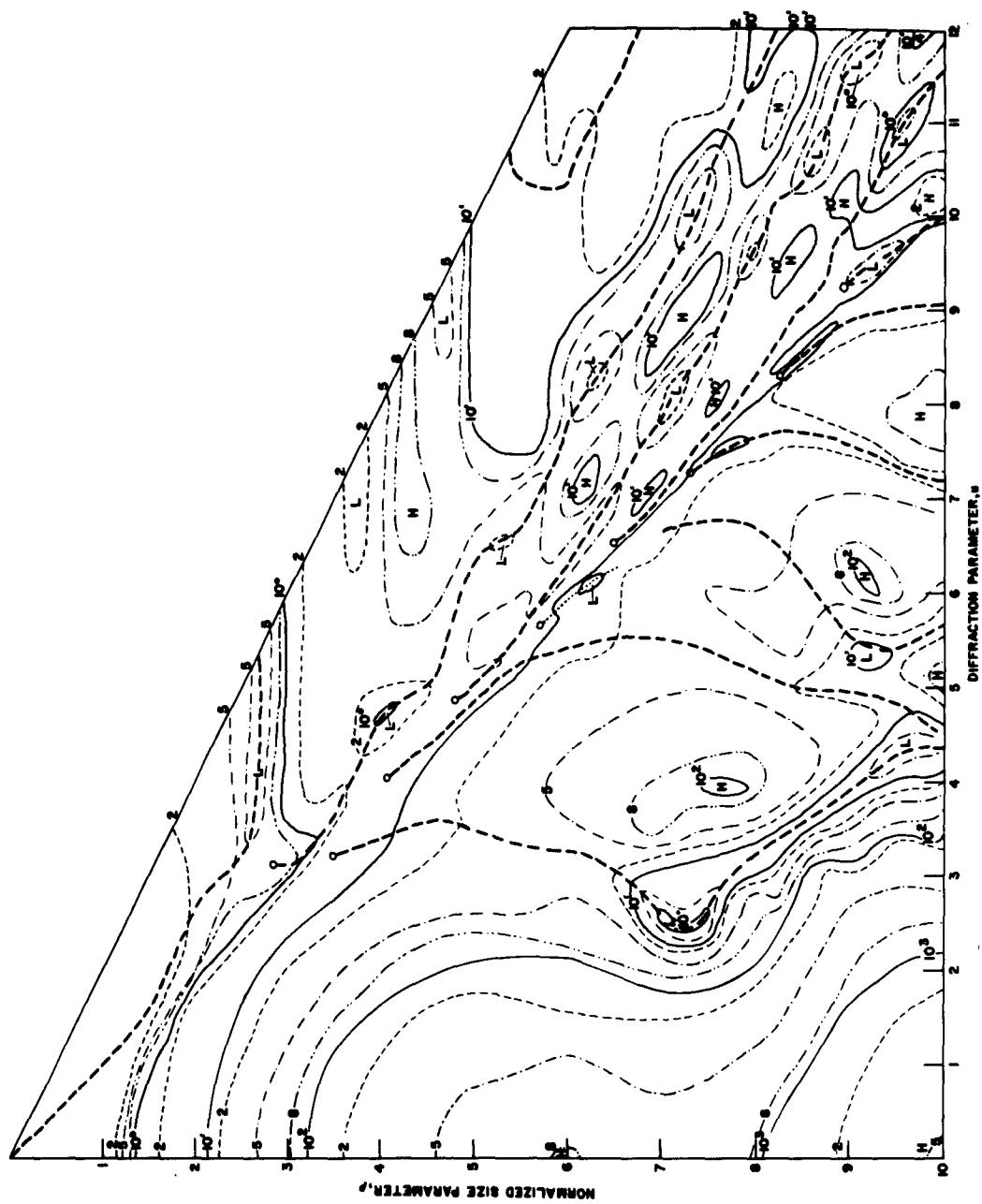


Figure 3-1 ALTITUDE CHART FOR INTENSITY FUNCTION i_1 AND $n = 1.5$ ($\rho < 10$)

Contours for i_1 are drawn in a quasi-logarithmic scale; namely, $1 \cdot 10^{-1}$, $2 \cdot 10^{-1}$, $5 \cdot 10^{-1}$, $8 \cdot 10^{-1}$, $1 \cdot 10^0$, $2 \cdot 10^0$, and so on. Heavy dashed lines represent position of dark rings. Open circles represent beginning of dark rings. Letters H (high) and L (low) represent peaks and trenches, respectively, of intensity function. For reason of clarity only, some contours, especially around $\theta = 900$, have been left out.

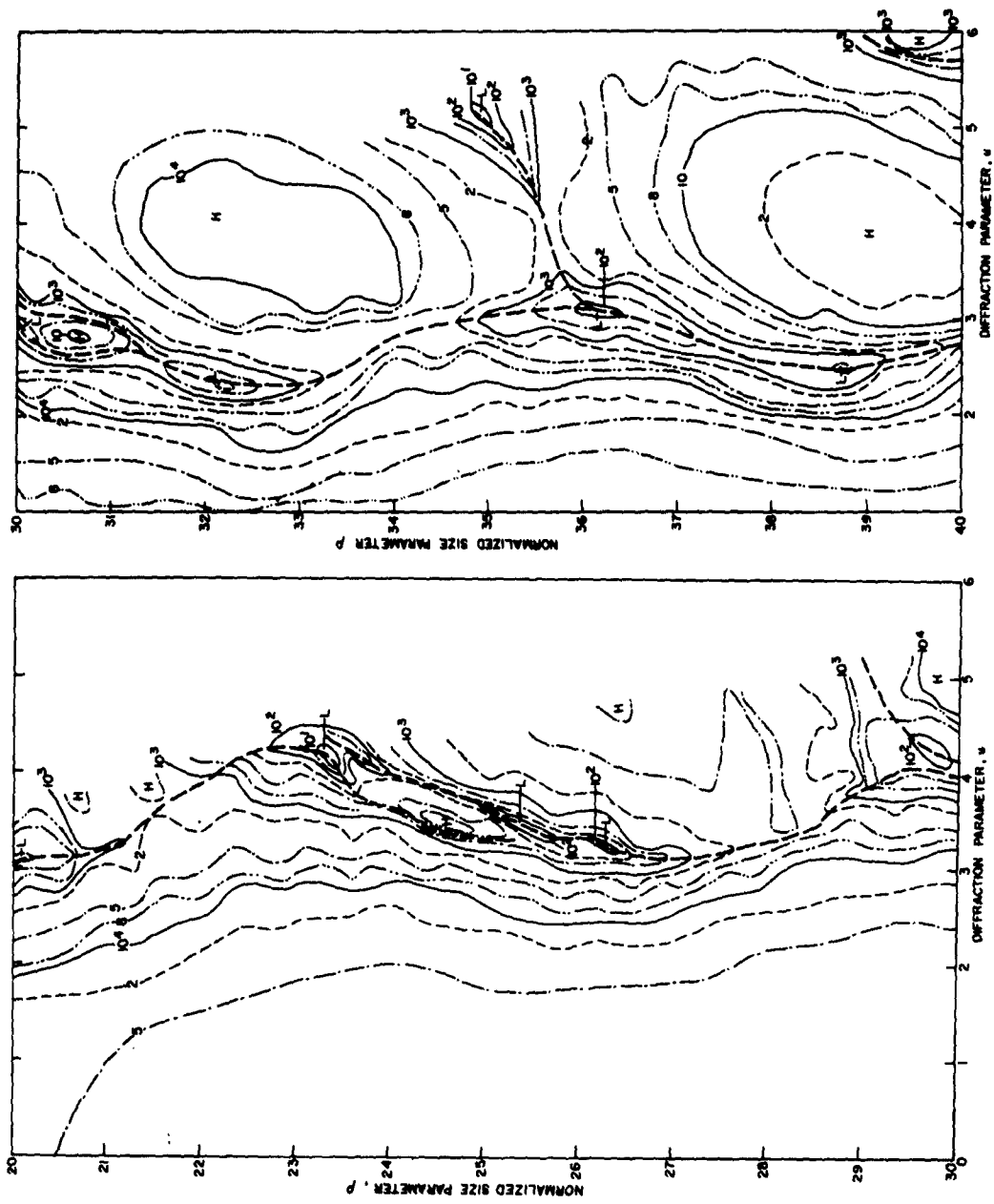


Figure 3-2 ALTITUDE CHART FOR INTENSITY FUNCTION i_1 AND
 $n = 1.5$ ($20 < p < 40$)

This chart represents the forward area for $\theta < 10$ only. The emphasis is placed on the first diffraction minimum, and some contours are left out.

63-3106

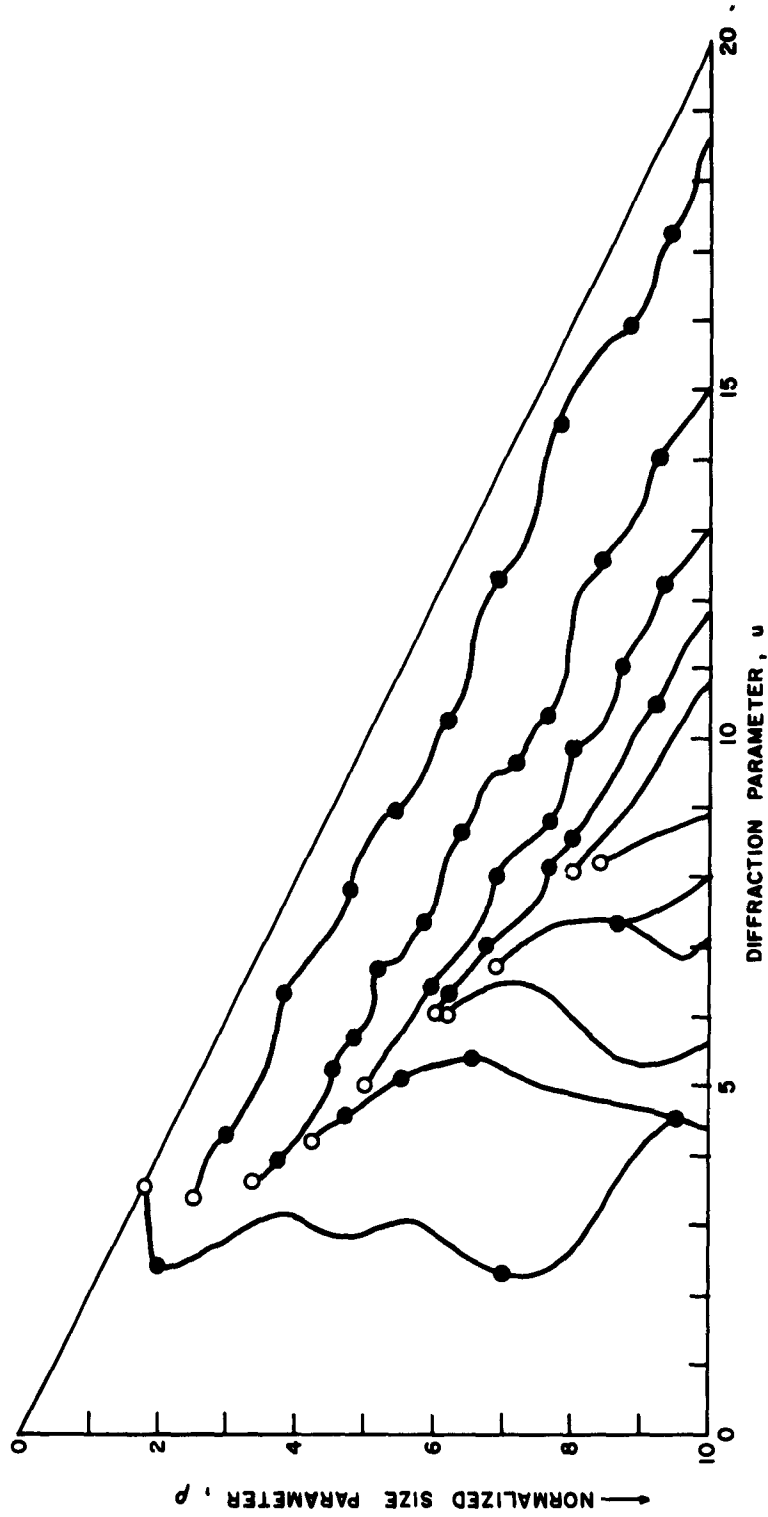


Figure 3-3a POSITION OF DARK RINGS AND CENTER OF TRENCHES
IN ALTITUDE CHART FOR INTENSITY FUNCTION i_1 AND $n = 1.5$

The position of the dark rings is indicated by solid lines. Open circles represent the beginning of a new ring. The center position of trenches is indicated by full circles.

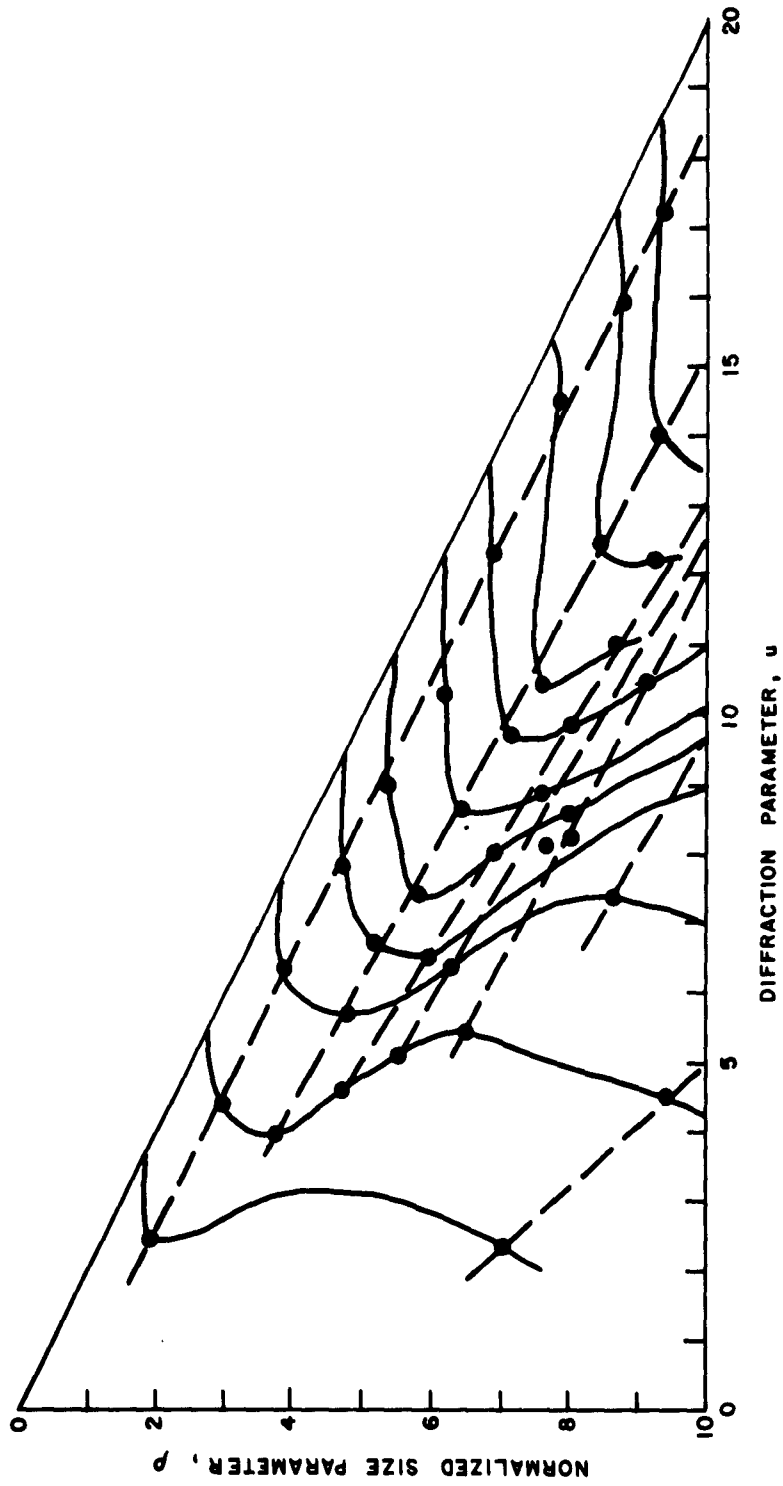


Figure 3-3b DIFFRACTION AND REFLECTION MINIMA FOR i_1 AND $n = 1.5$

The two systems as explained in the text are shown. A solid line represents the diffraction minima, a dashed line the reflection minima. The center position of trenches is indicated by full circles.

63-3083



Figure 3-4 ALTITUDE CHARTS FOR INTENSITY FUNCTION i_2 AND $n = 1.5$

Contours for i_2 are drawn in a quasi-logarithmic scale; namely, $1 \cdot 10^{-1}$, $2 \cdot 10^{-1}$, $5 \cdot 10^{-1}$, $8 \cdot 10^{-1}$, $1 \cdot 10^0$, $2 \cdot 10^0$, and so on. Heavy dashed lines represent position of dark rings. Open circles represent beginning of dark rings. Letters H (high) and L (low) represent peaks and trenches, respectively, of intensity function. For reason of clarity only, some contours, especially around $\theta = 90^\circ$, have been left out.

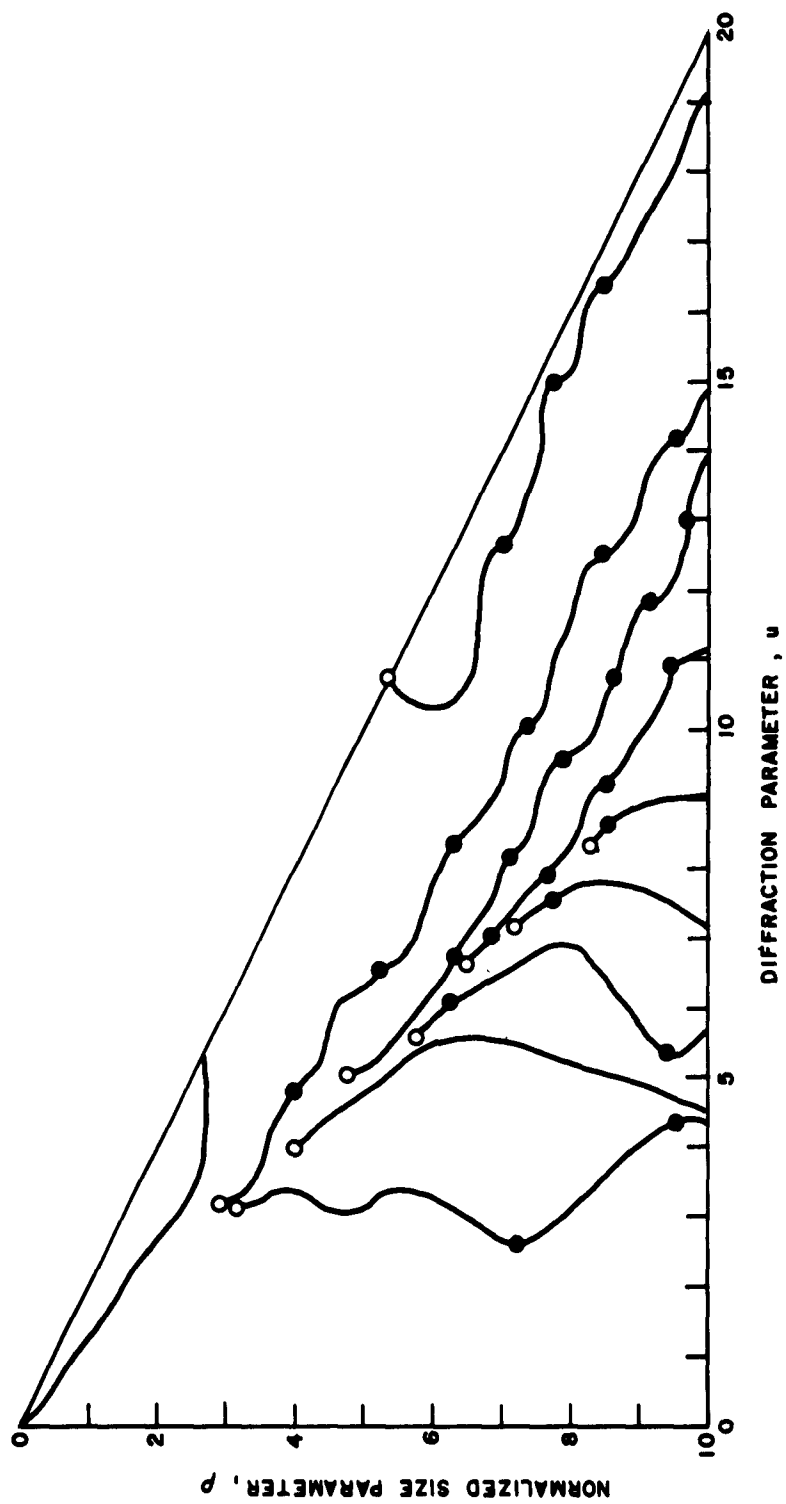


Figure 3-5a POSITION OF DARK RINGS AND CENTER OF TRENCHES IN ALTITUDE CHART FOR INTENSITY FUNCTION i_2 AND $n = 1.5$

The position of the dark rings is indicated by solid lines. Open circles represent the beginning of a new ring. The center position of trenches is indicated by full circles.

63-3082

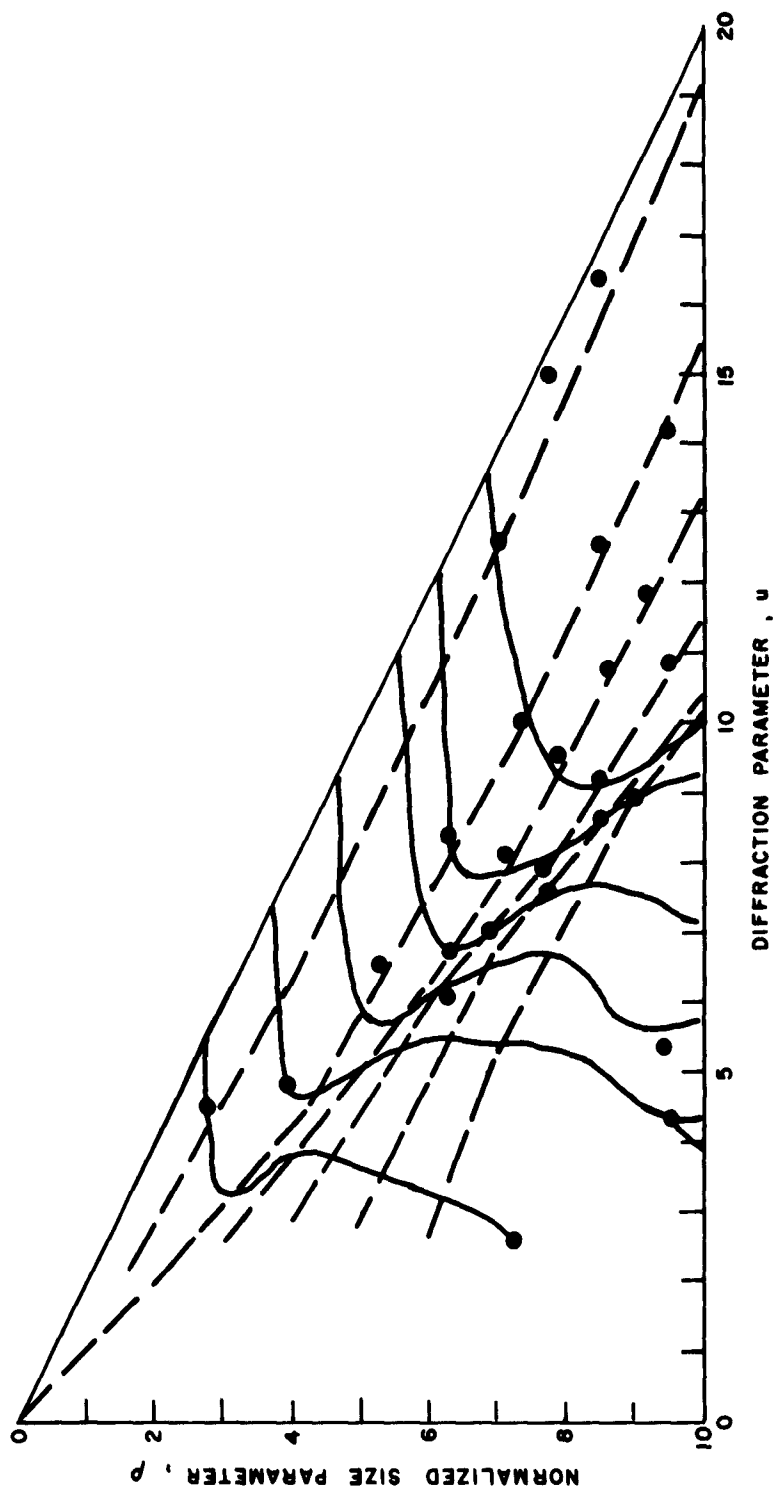


Figure 3-5b DIFFRACTION AND REFLECTION MINIMA FOR i_2 AND $n = 1.5$

The two systems as explained in the text are shown. A solid line represents the diffraction minima, a dashed line the reflection minima. The center position of trenches is indicated by full circles.

63-3081

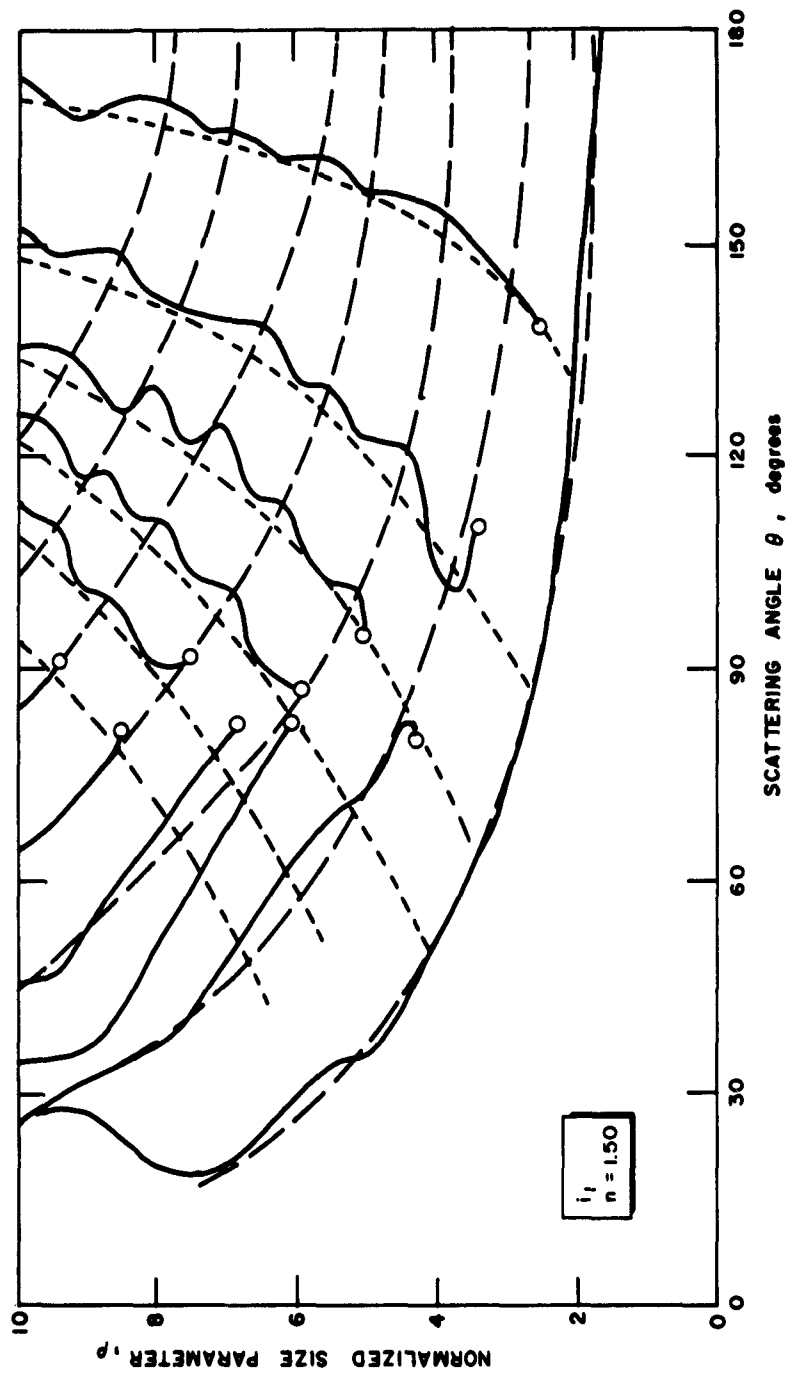


Figure 3-6 ANGULAR POSITION OF DARK RINGS FOR INTENSITY FUNCTION i_1
AS FUNCTION OF SIZE PARAMETER α FOR $n = 1.5$

Heavy lines show the position of the dark rings taken from the altitude chart. The diffraction minima system is indicated by thin dashed lines and the reflection minima system by thin dotted lines.

60-3079

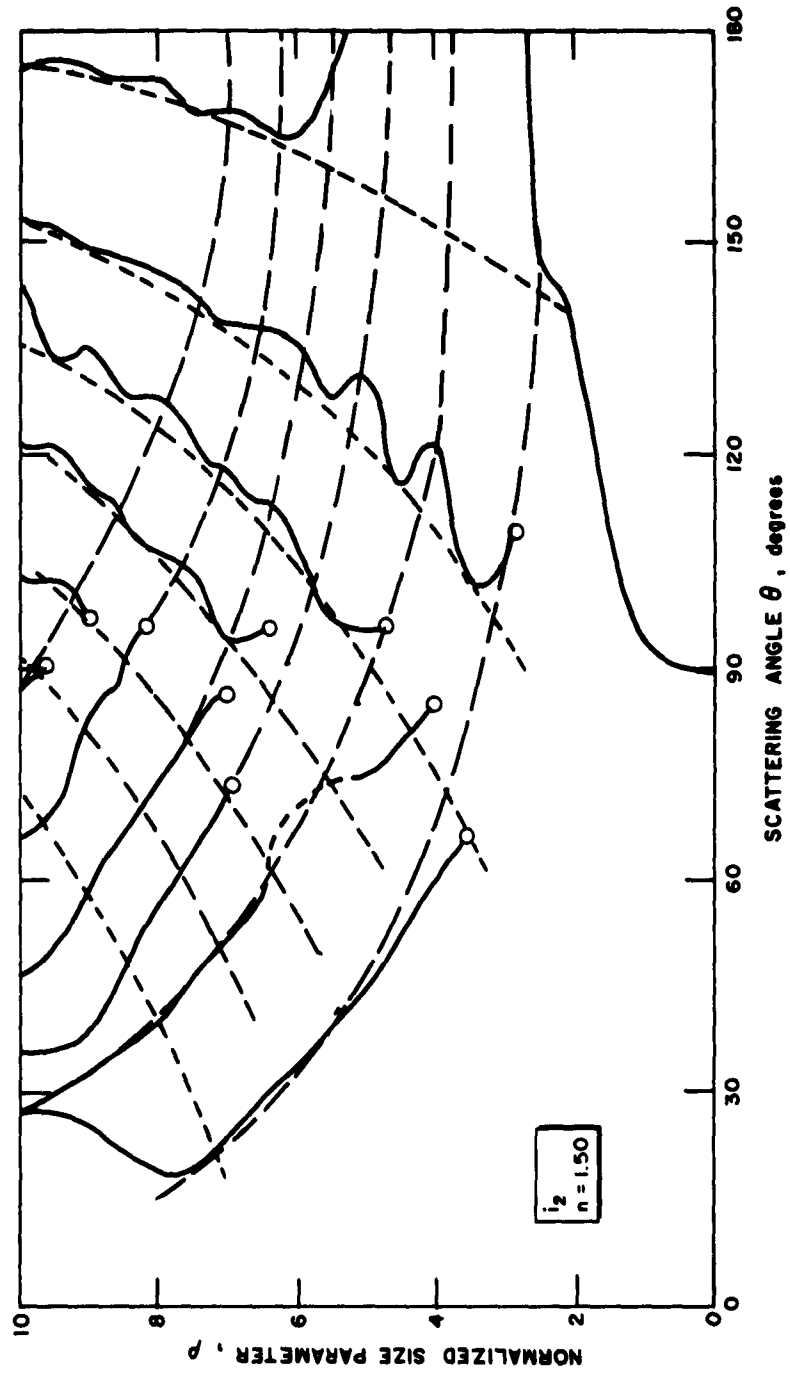


Figure 3-7 ANGULAR POSITION OF DARK RINGS FOR INTENSITY FUNCTION i_2
AS FUNCTION OF SIZE PARAMETER α FOR $n = 1.5$

Heavy lines show the position of the dark rings taken from the altitude chart. The diffraction minima system is indicated by thin dashed lines and the reflection minima system by thin dotted lines.

63-3080

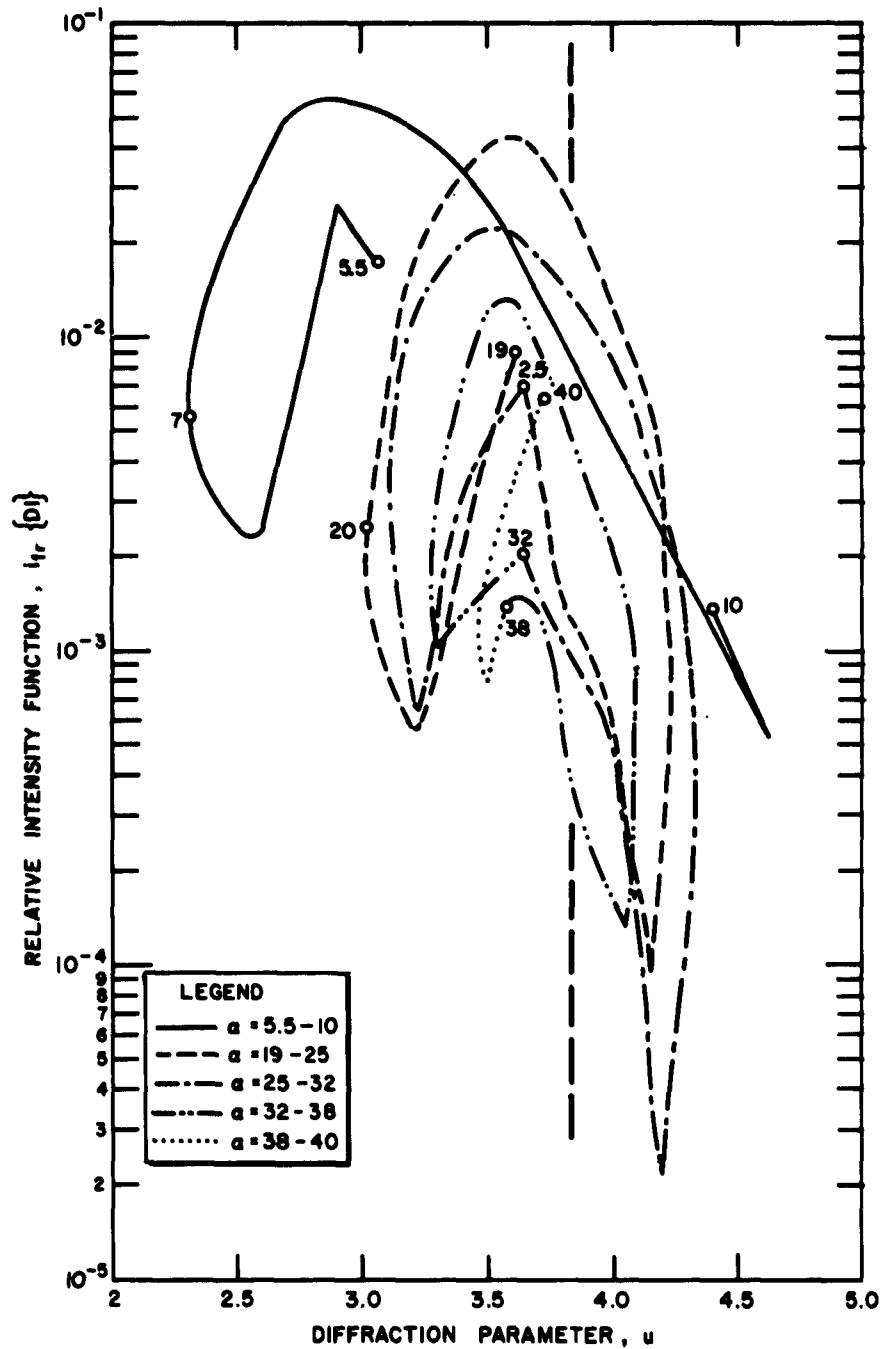


Figure 3-8 RELATIVE INTENSITY FUNCTION i_{1r} FOR THE FIRST DIFFRACTION MINIMUM AS FUNCTION OF DIFFRACTION PARAMETER u FOR $n = 1.5$

Minima are reached when u approaches extreme values. Numbers on curve represent selected α values. Data are based on altitude charts prepared up to $\alpha = 40$. Heavy dashed line represents $u = 3.83$, the classical value for the first diffraction minimum.

63-3085

IV. CONCLUSIONS

Twenty scattering diagrams of the intensity functions i_1 , i_2 , and $i_1 + i_2$ are given in the form of an atlas for $n = 1.5$ and $\alpha = 0.5 (0.5) 10$. They are based on computations in steps of $\Delta\alpha = 0.1$ and $\theta = 0 (1) 10 (10) 180^\circ$.

Since a linear interpolation is not allowable for $\alpha > 3$, interpolation methods have been investigated. The altitude-chart technique allows to interpolate the functions graphically for any set of $\alpha - \theta$ values. Furthermore, the position and depth of the minima are determined correctly. The dark rings may clearly be divided into the two groups: those due to diffracted light, and those due to reflected and refracted light. For the first group, the diffraction parameter u for each particular dark ring meanders around the classical diffraction parameter which it approaches asymptotically for very large spheres. For the second group, the diffraction parameter u increases proportional to ρ . The center of the deep trenches occur for the first group in steps of $\Delta\rho \approx \pi$, for the second group in steps of $\Delta\rho = 0.81$. The two systems can be separated, and the interaction of the two systems determines the direction in which the predominant minimum moves. This interaction also explains the position of the trenches and the areas where the minima suddenly become indistinguishable.

The scattering diagrams have been constructed using all available interpolation techniques in addition to the computed data and represent the most reliable data up to $\alpha = 10$. They allow interpolation for any set of $\alpha - \theta$ values.

V. BIBLIOGRAPHY

- Giese, R. H., E. deBary, K. Bullrich, and C. D. Vinnemann, Tabellen der Streufunktionen i_1 , i_2 und des Streuquerschnittes homogener Kuegelchen nach der Mie'schen Theorie, Abh. Deutsche Akad. Wissensch. Berlin Klasse Math. Phys. Techn. 1961 (6) (1962), 175 p.
- Olaf, J. and K. Robock, Zur Theorie der Lichtstreuung an Kohle- und Bergepartikeln, Staub 21, 495 (1961).
- Penndorf, R. and B. Goldberg, Tables of Light Scattering Functions, unpublished manuscript (1953).
- Penndorf, R., [An] Approximate method to the Mie theory for colloidal spheres, J. Phys. Chem. 62, 1537 (1958).
- Penndorf, R., Bright and Dark Rings, AFCRL-425, Avco RAD-TR-61-16 (1961a).
- Penndorf, R., Atlas of Scattering Diagrams for $n = 1.33$, AFCRL-1044, Avco RAD-TR-61-32 (1961b).
- Robock K., Grundlagen der optischen Staubmessung, Staub 22, 80 (1962).
- Rowell, R., private communication (1962).
- van de Hulst, H. C., Light Scattering by Small Particles, Wiley, New York (1957), 470 p.

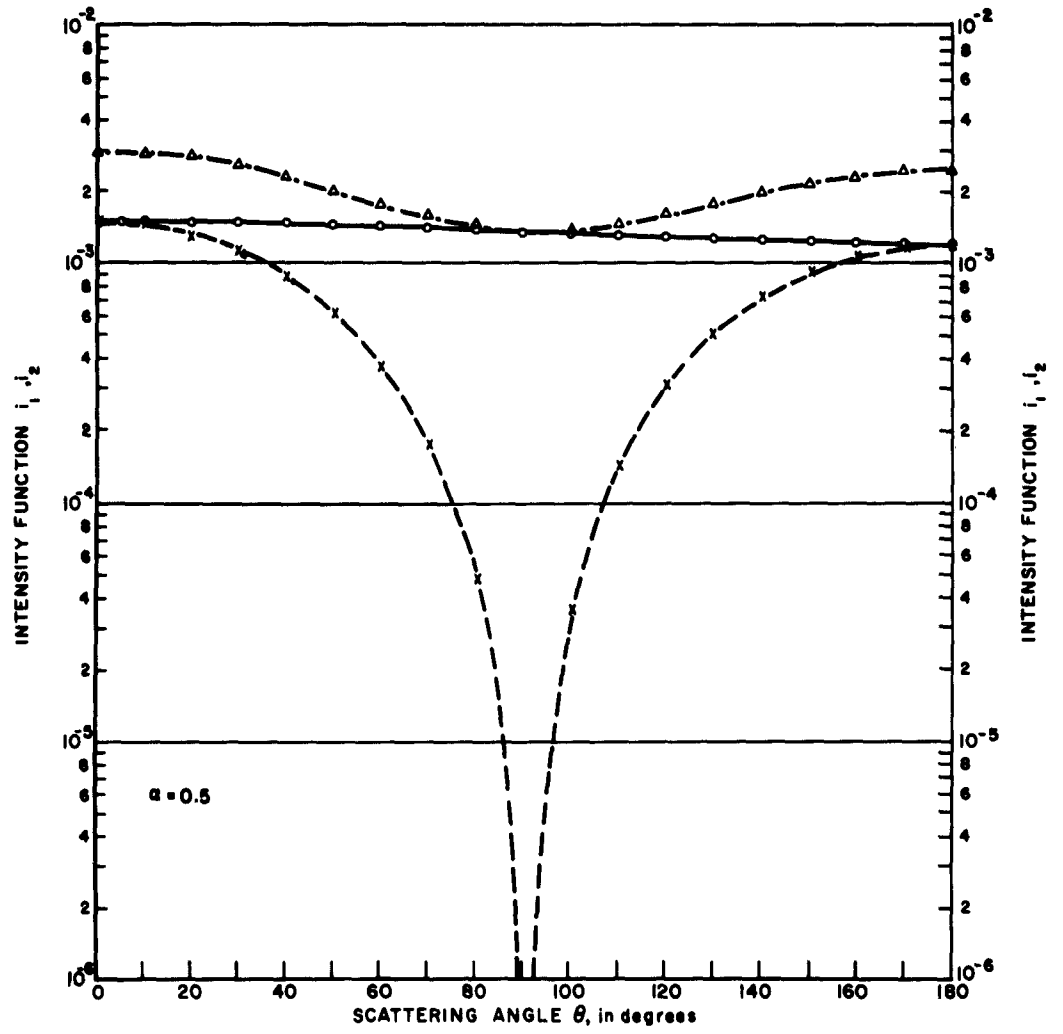
VI. APPENDIXES

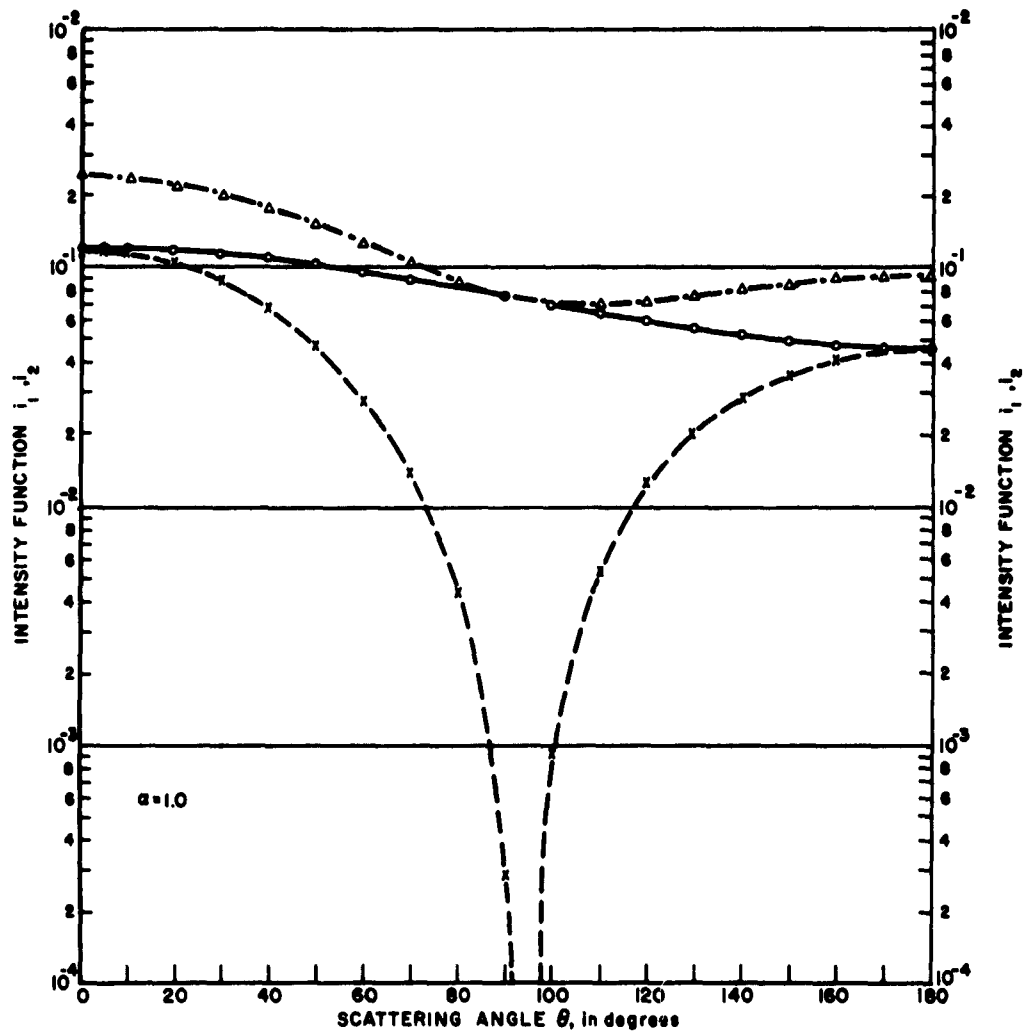
6.1 ATLAS

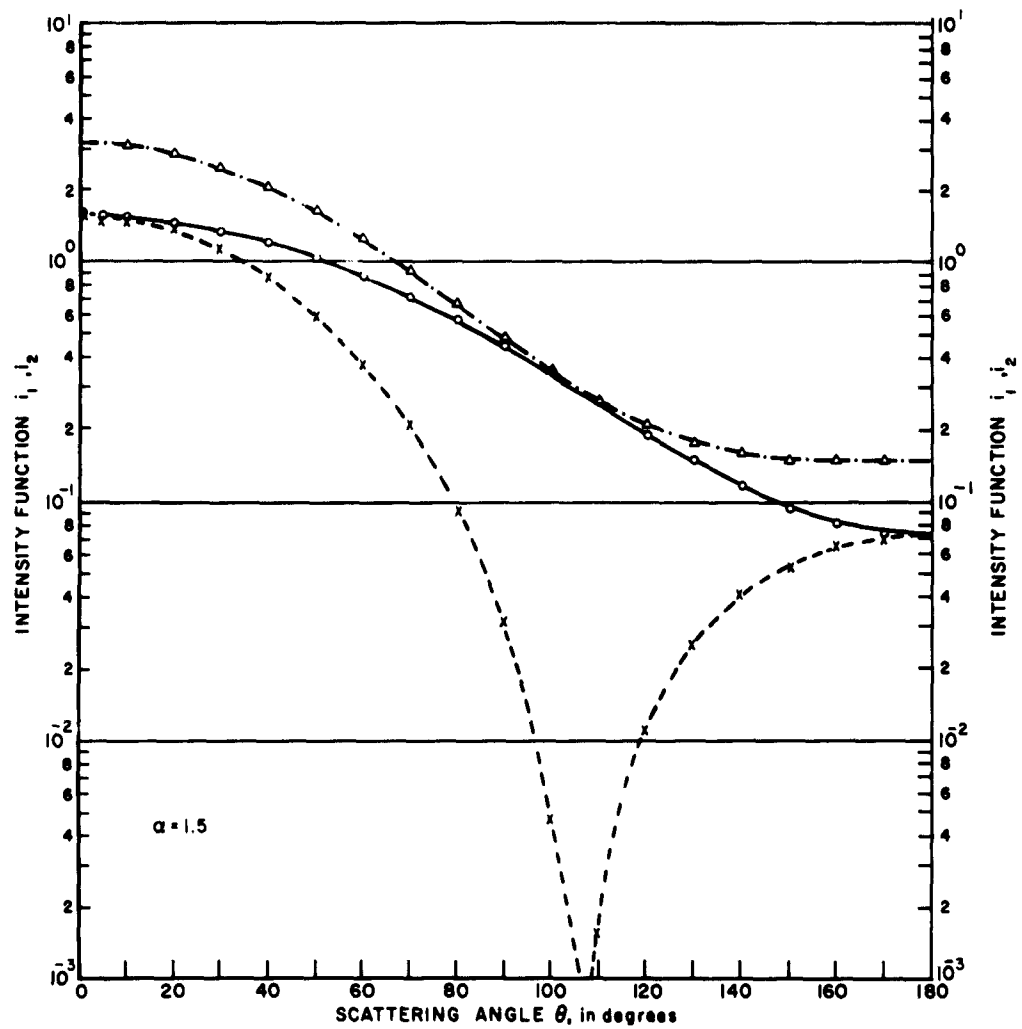
i_1 _____

i_2 _____

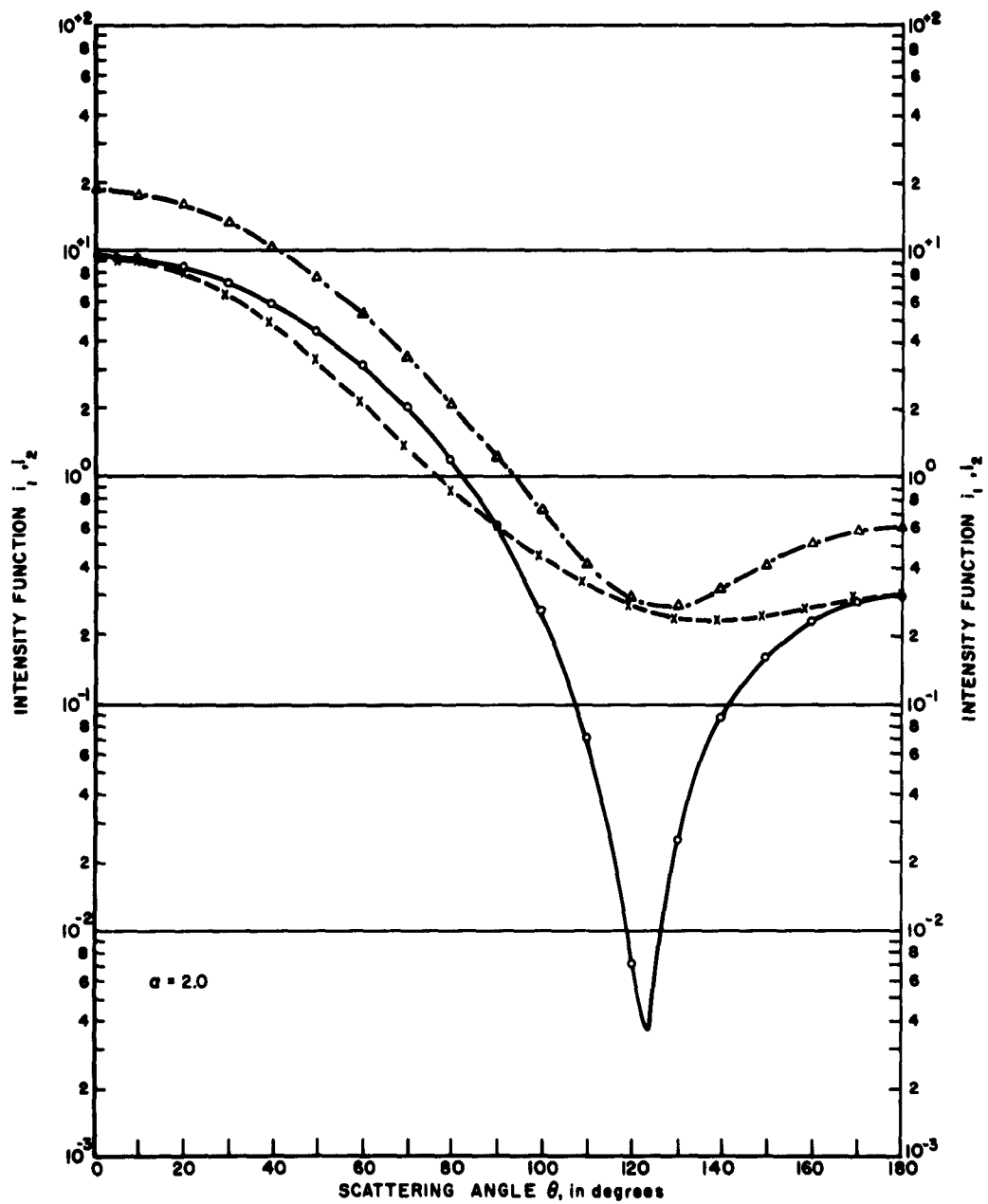
$i_1 + i_2$ - . - . - . - . - .

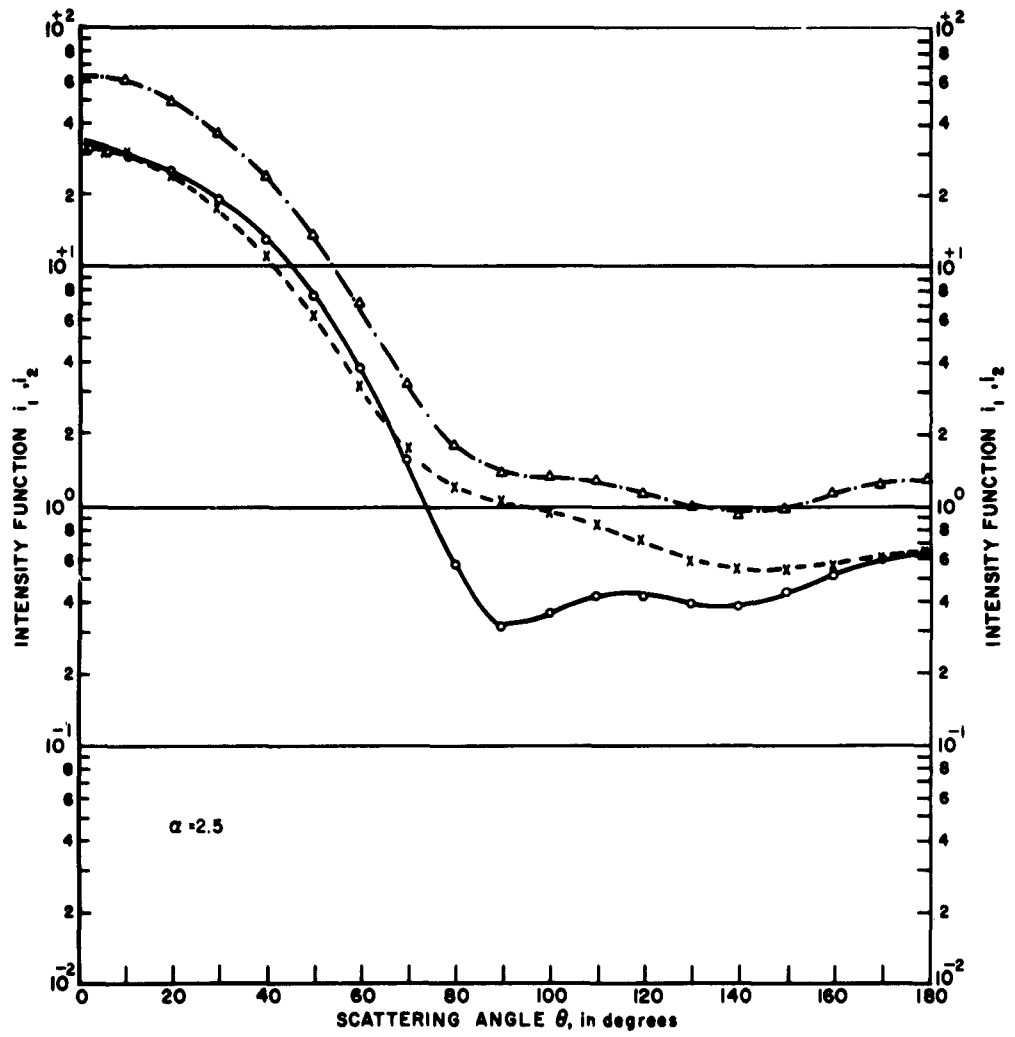




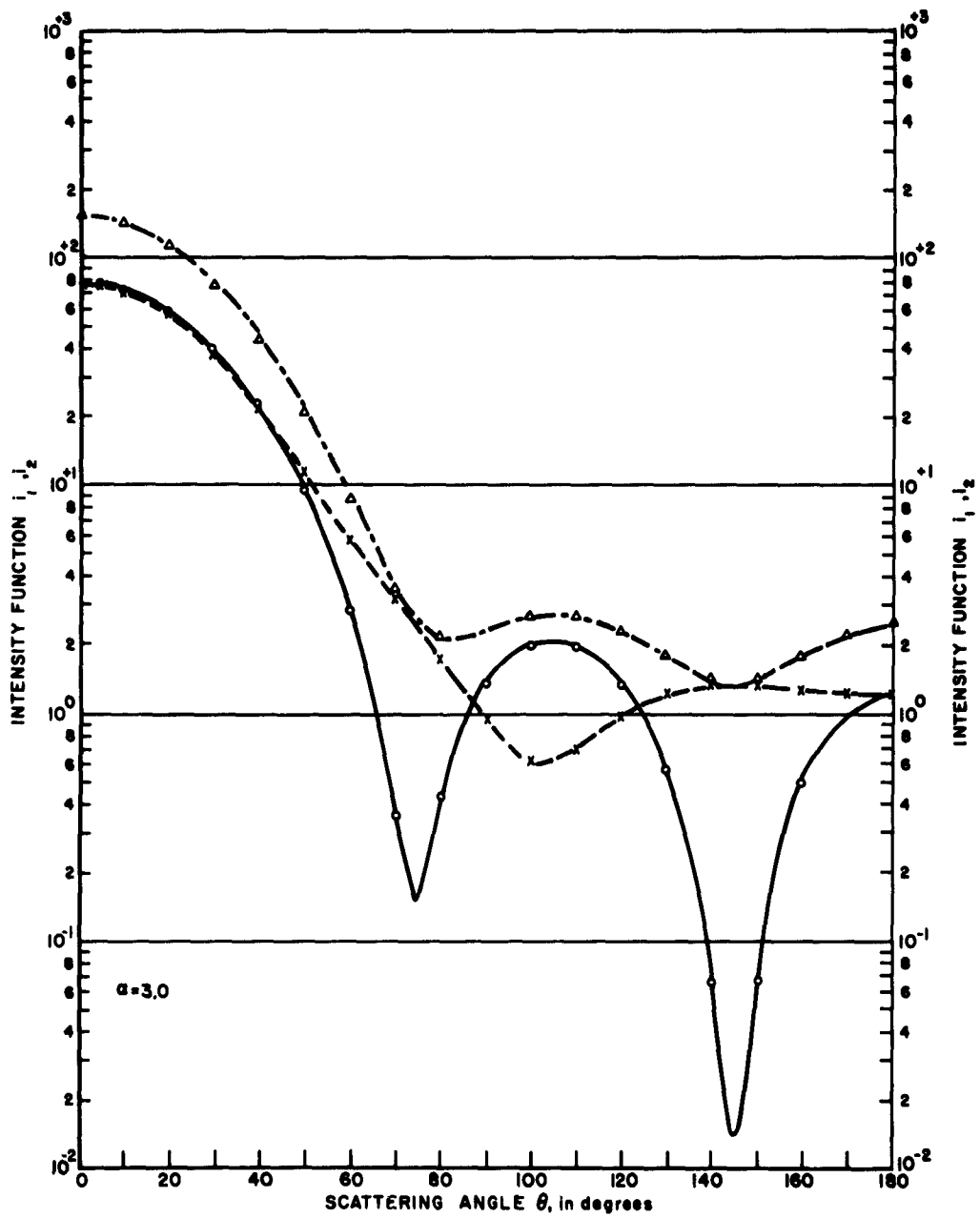


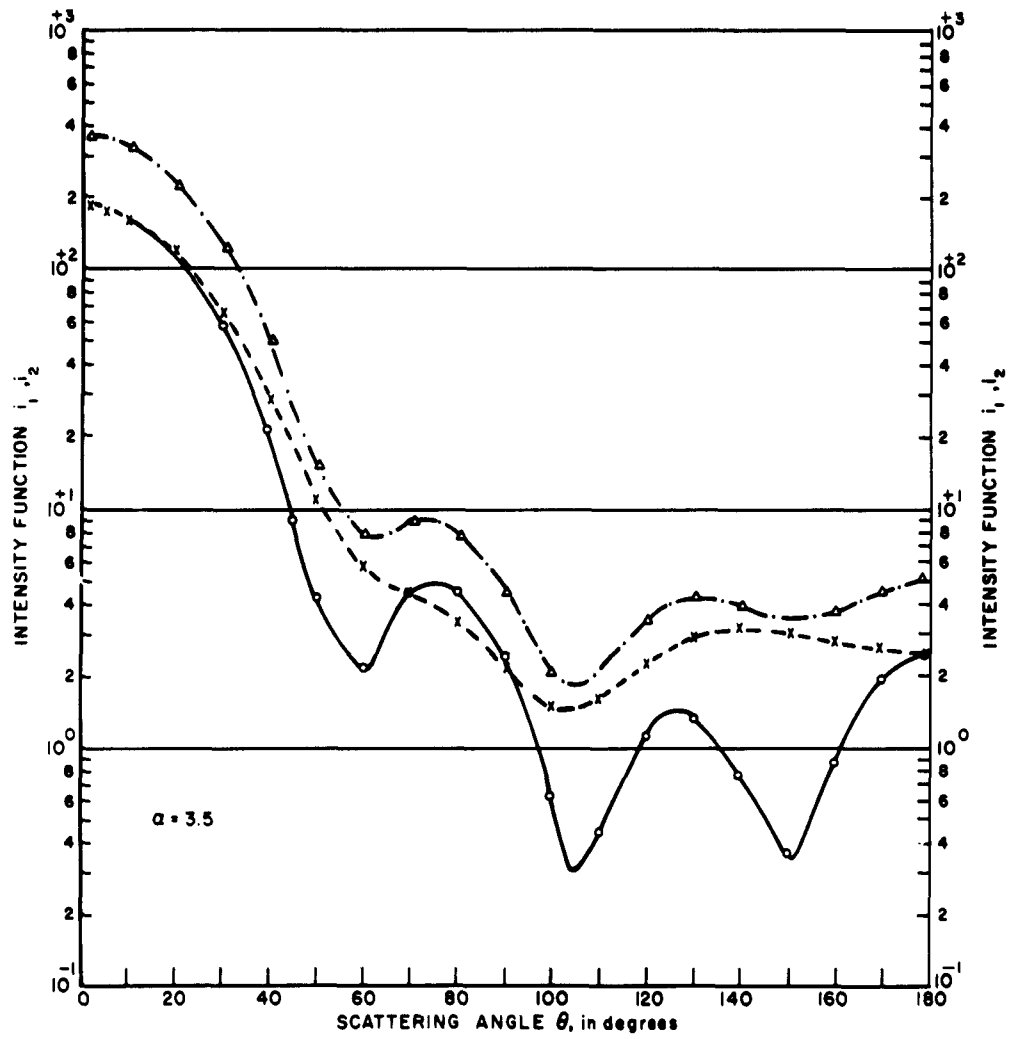
63-3088



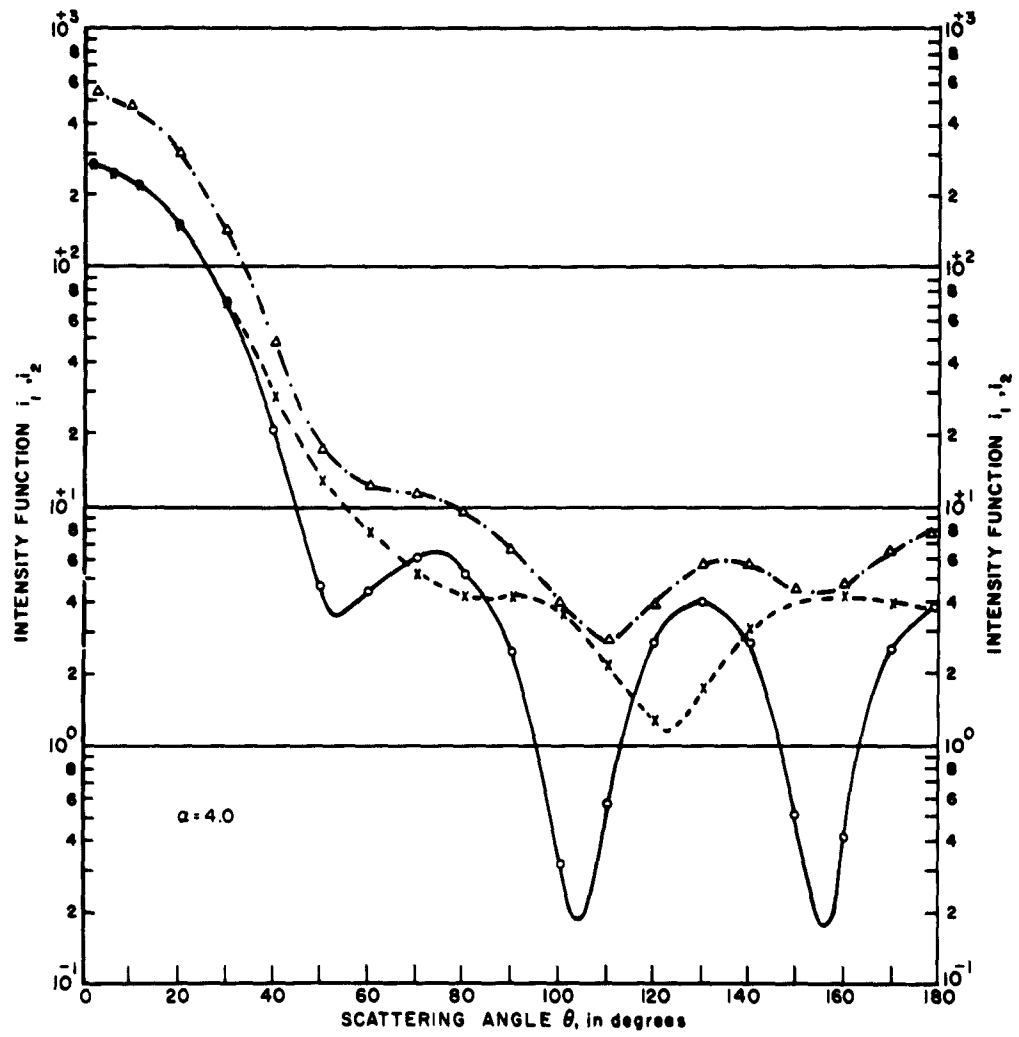


63-3080

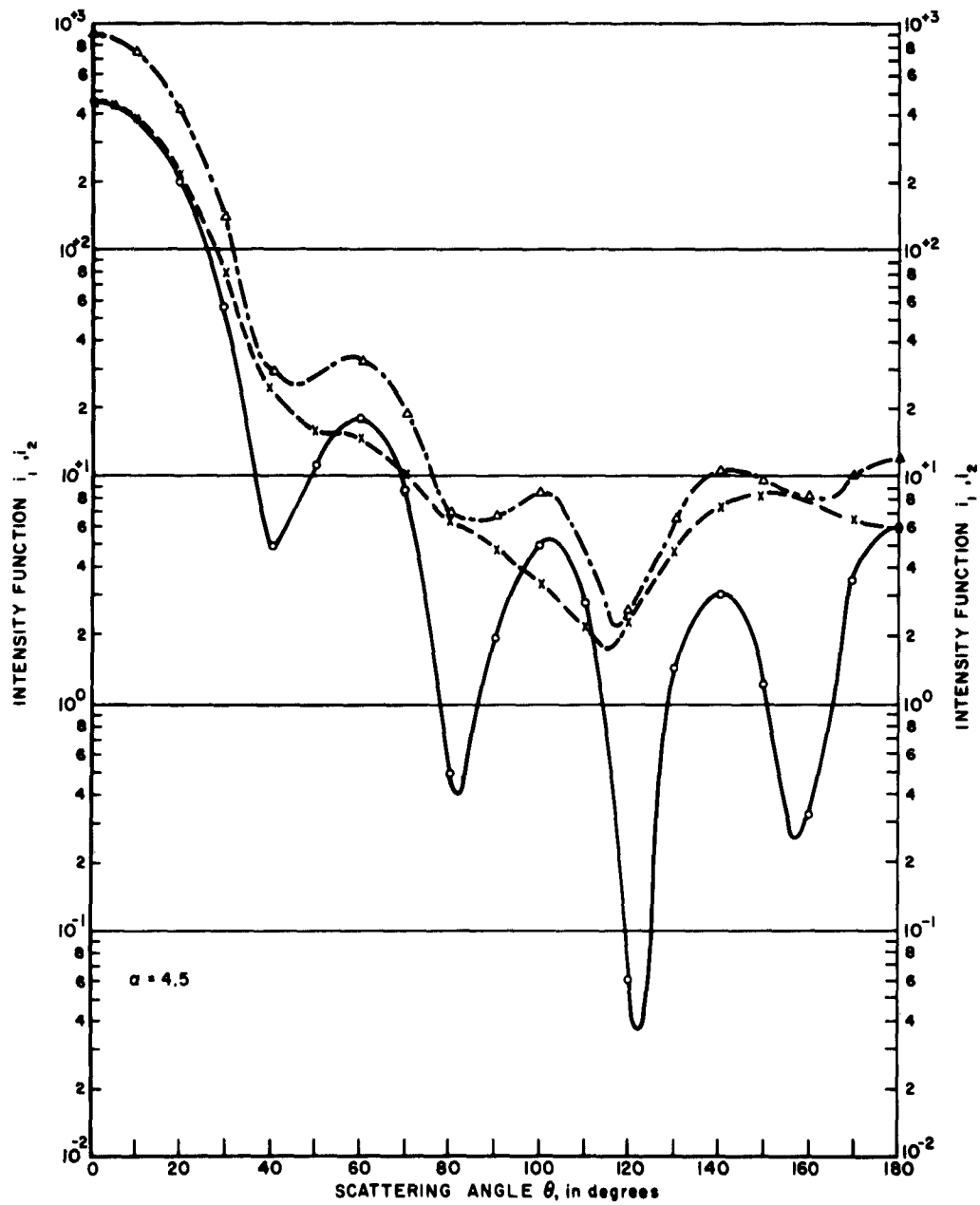


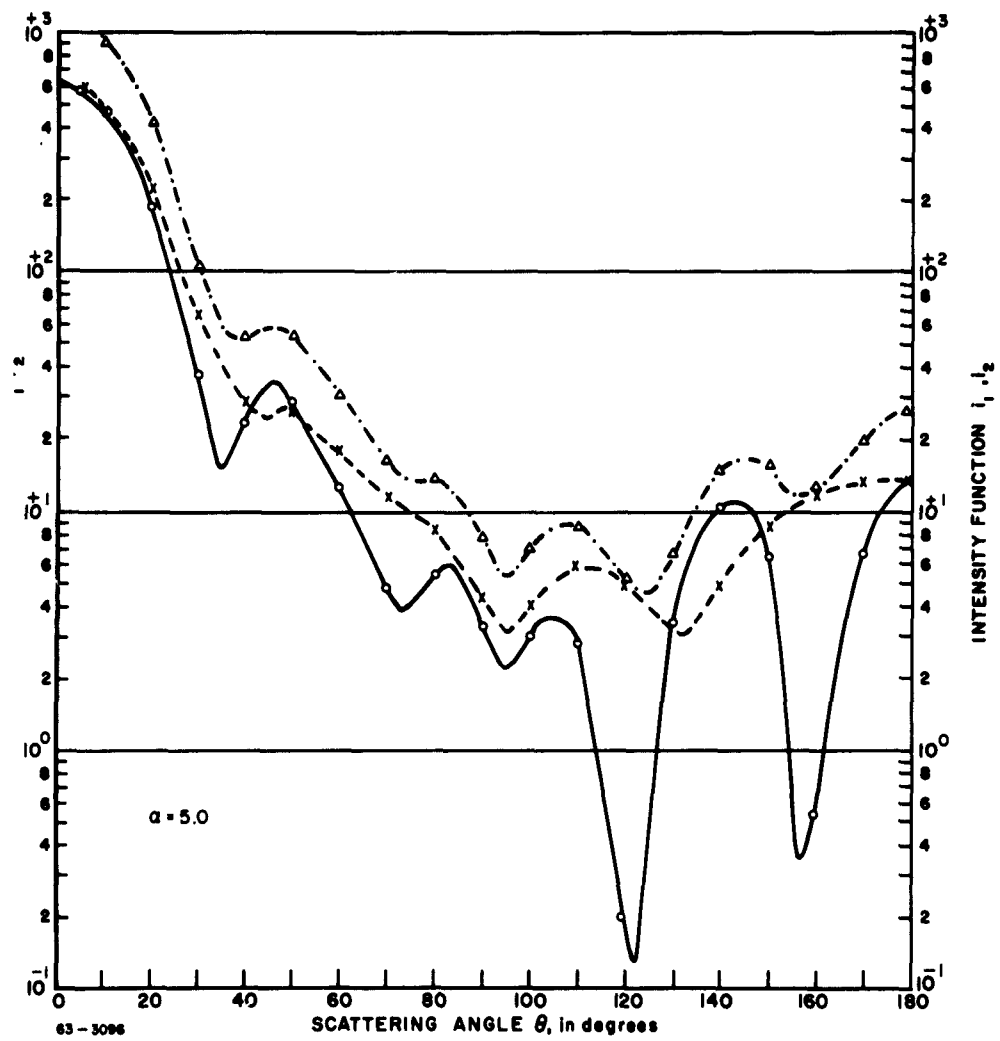


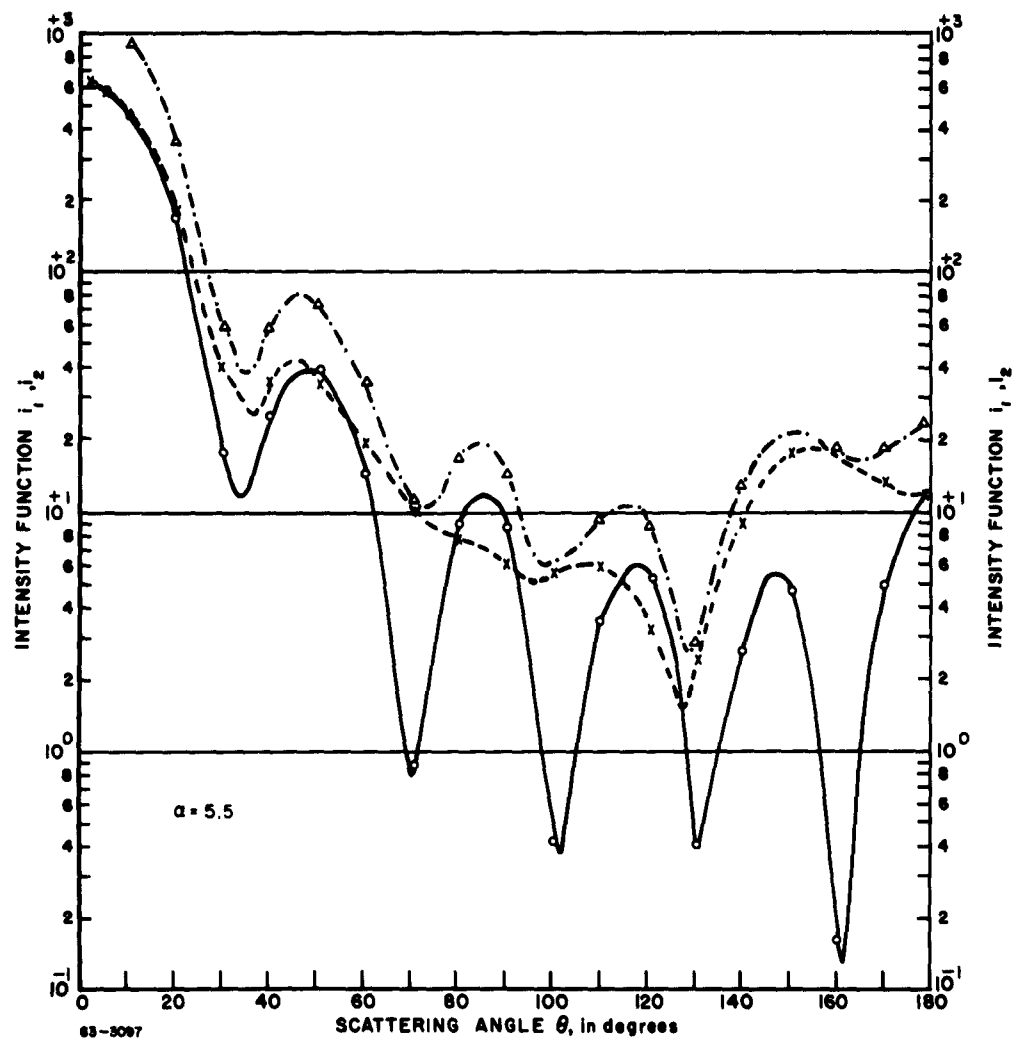
63-3092

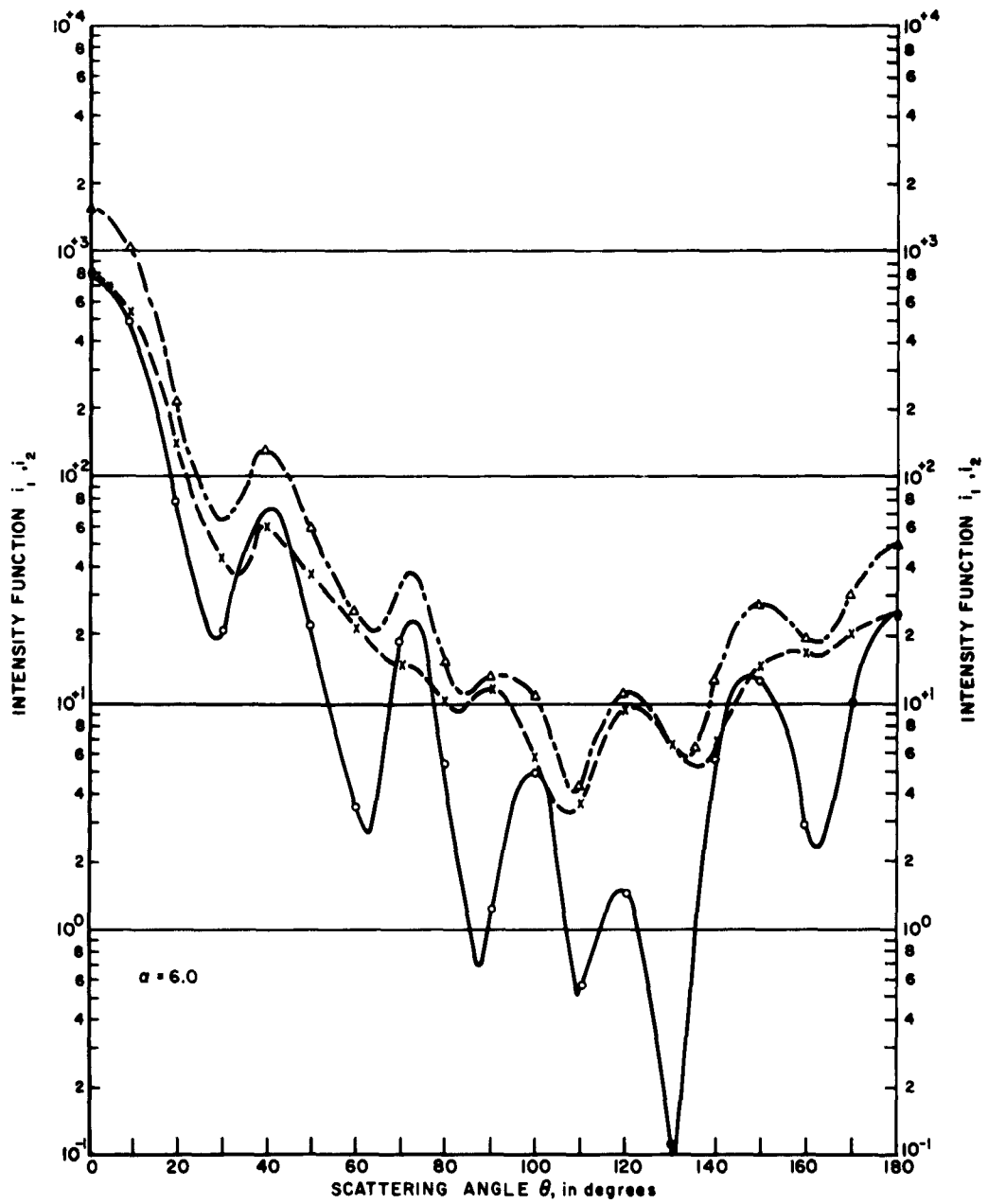


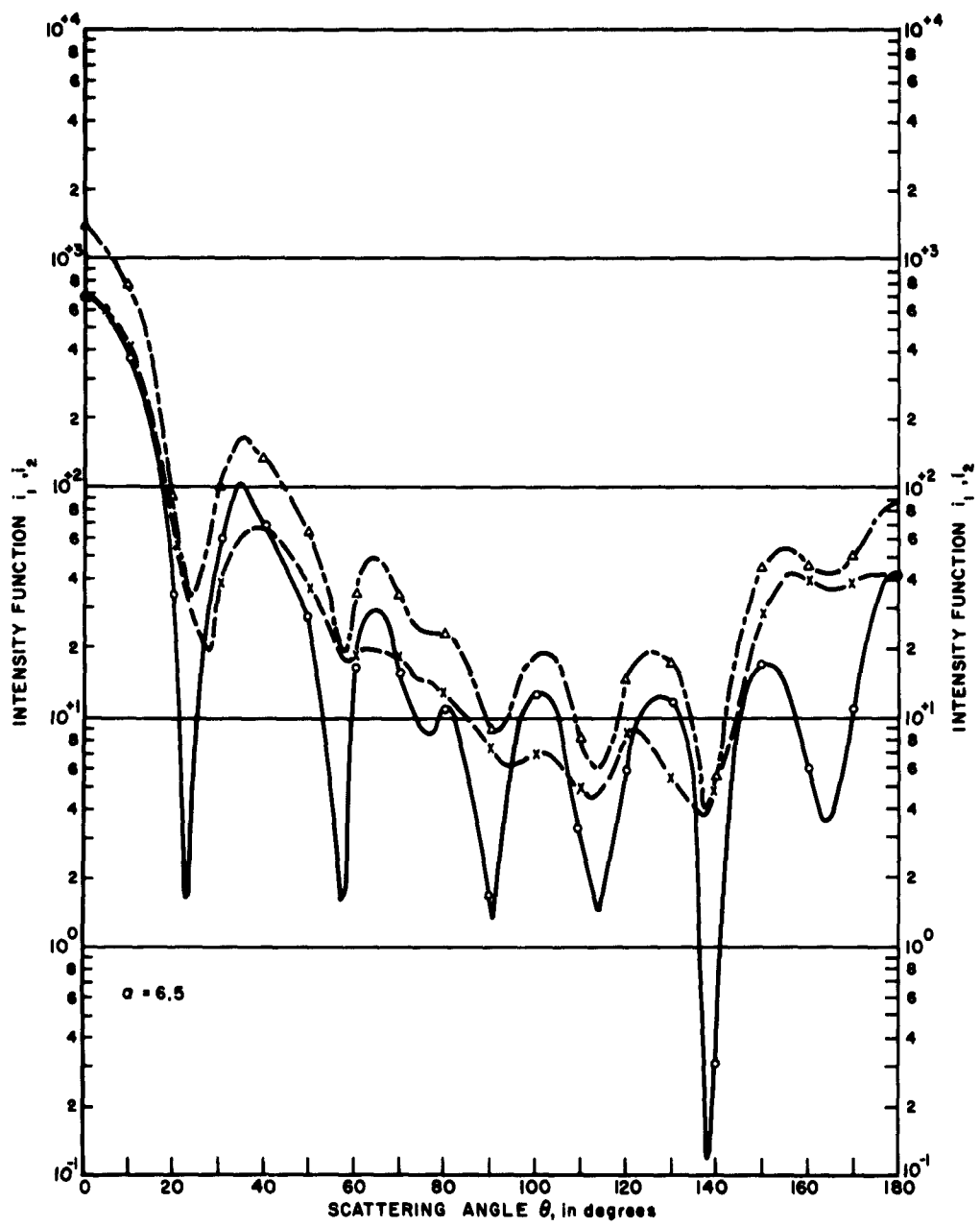
63-3094

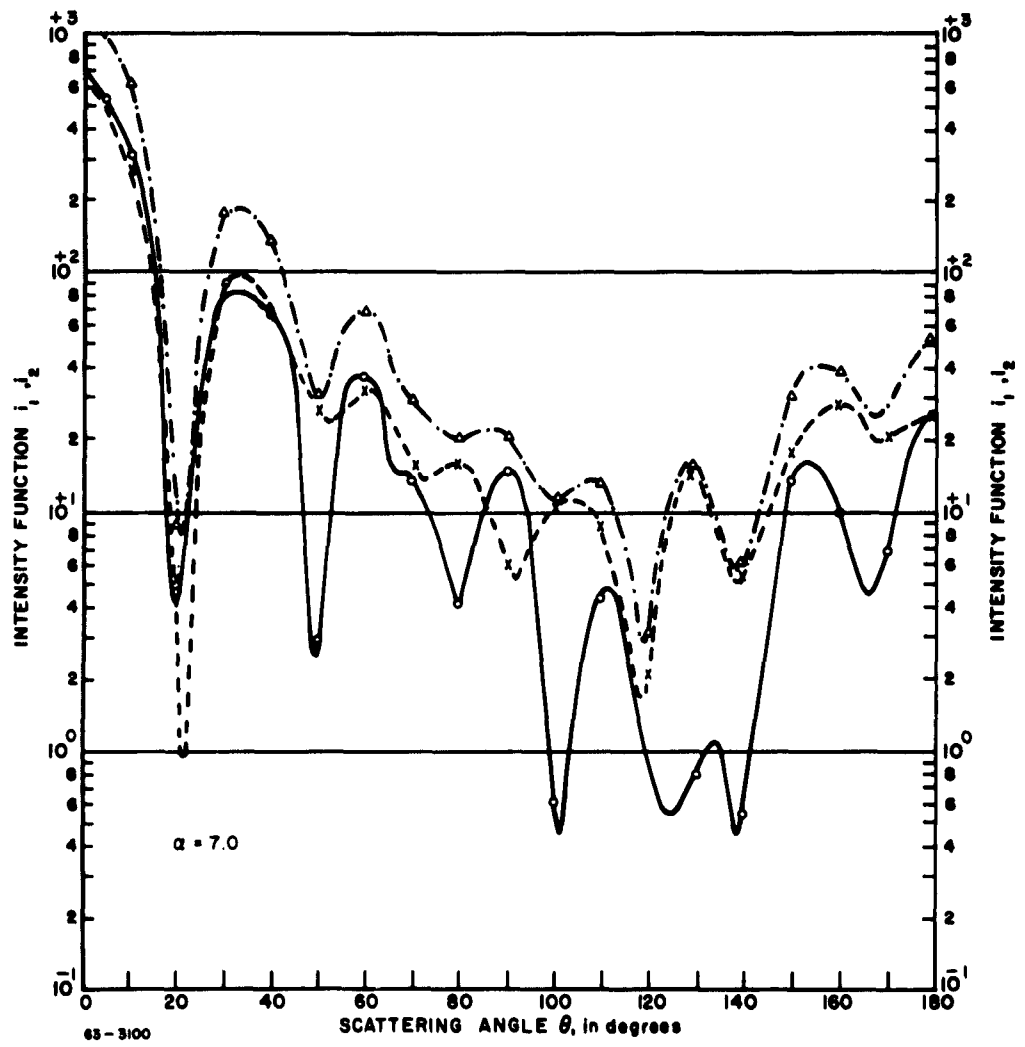


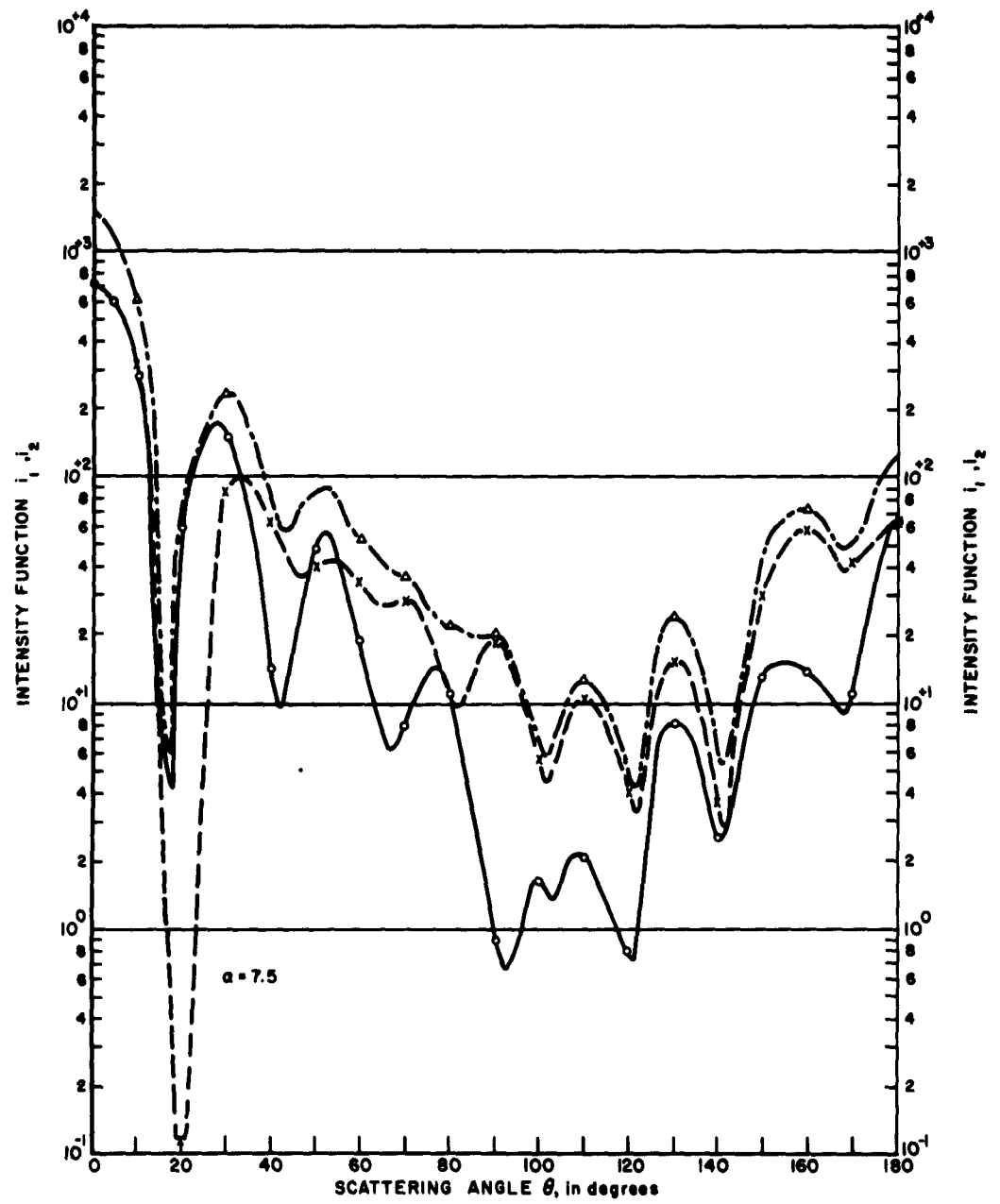


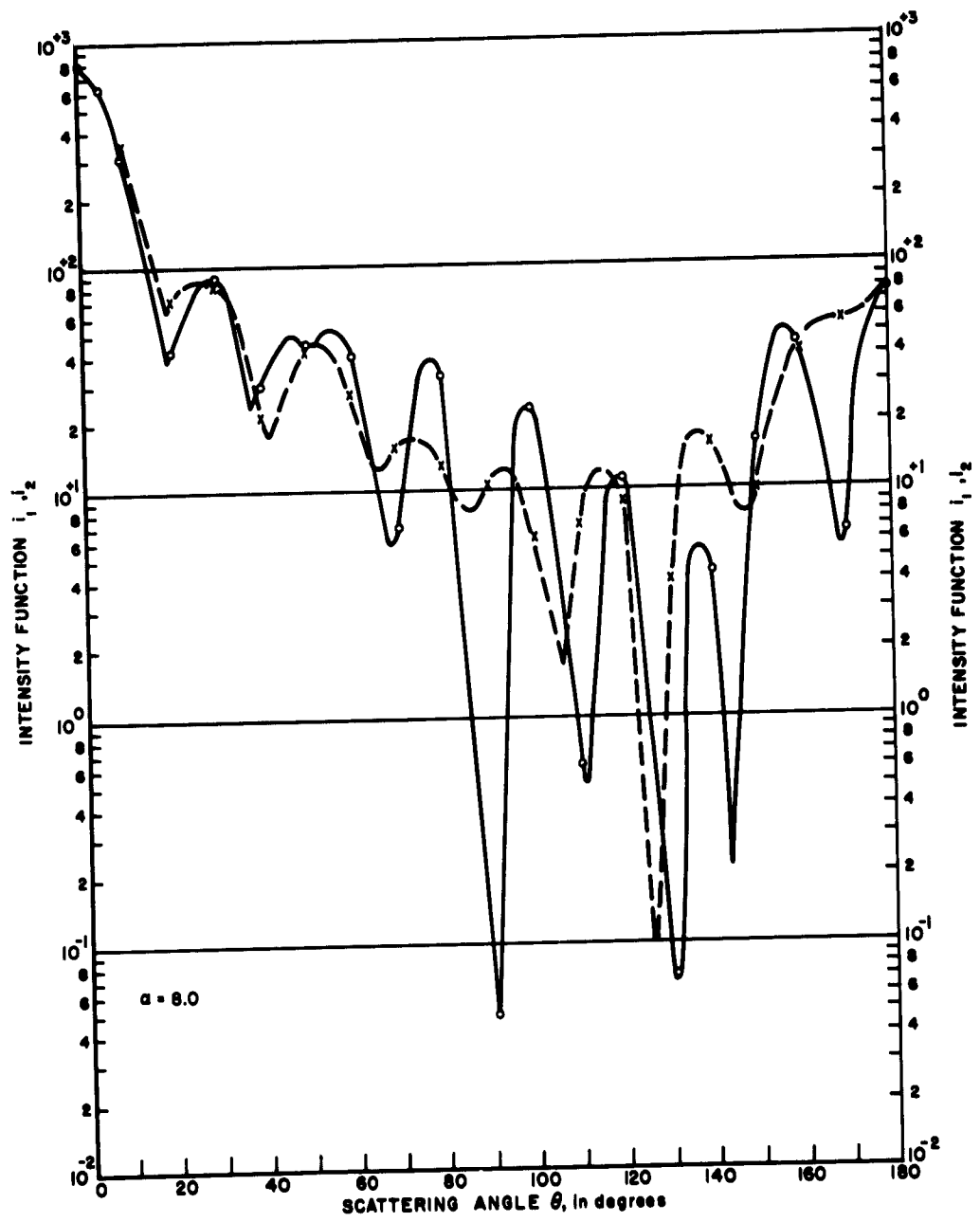


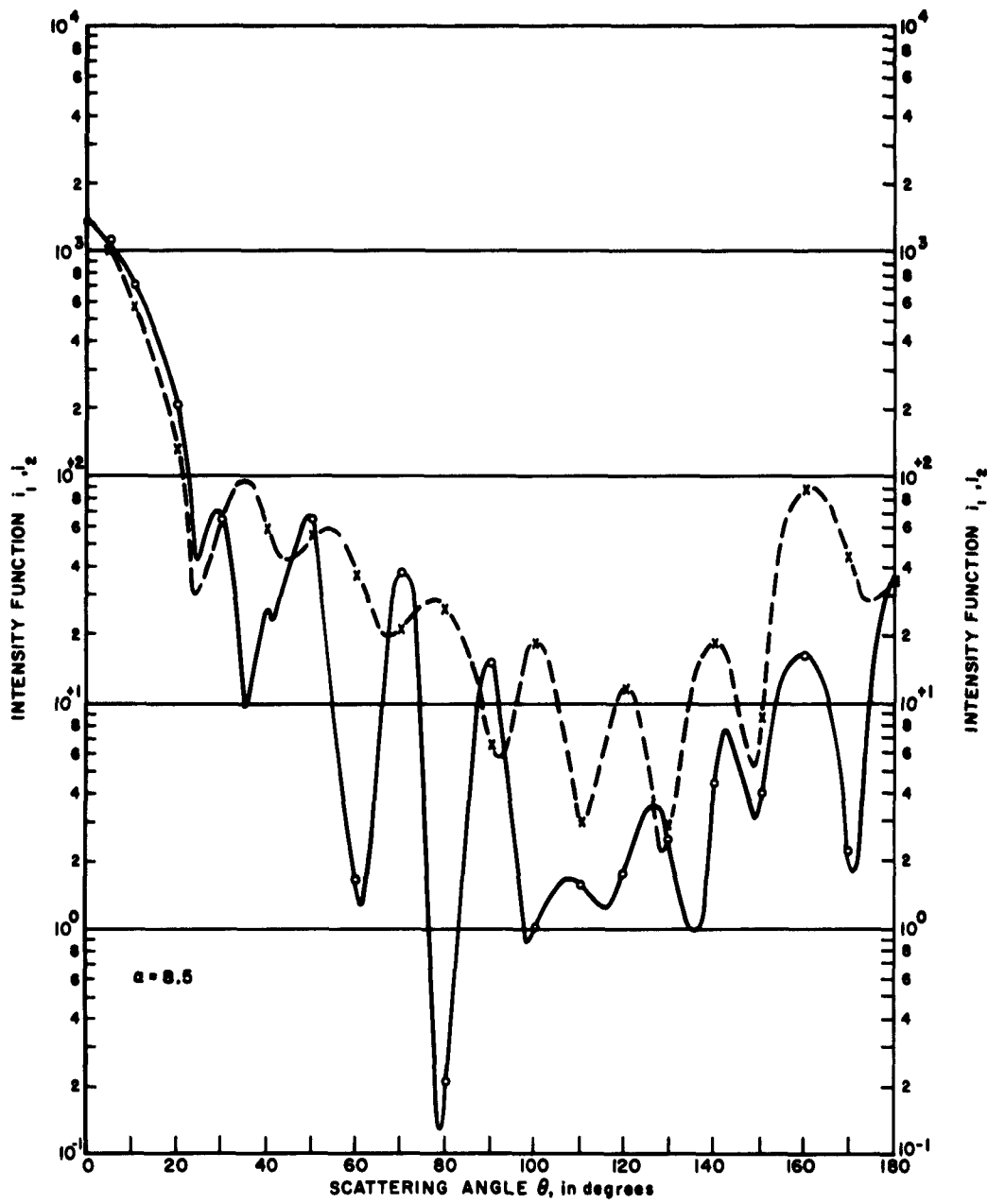


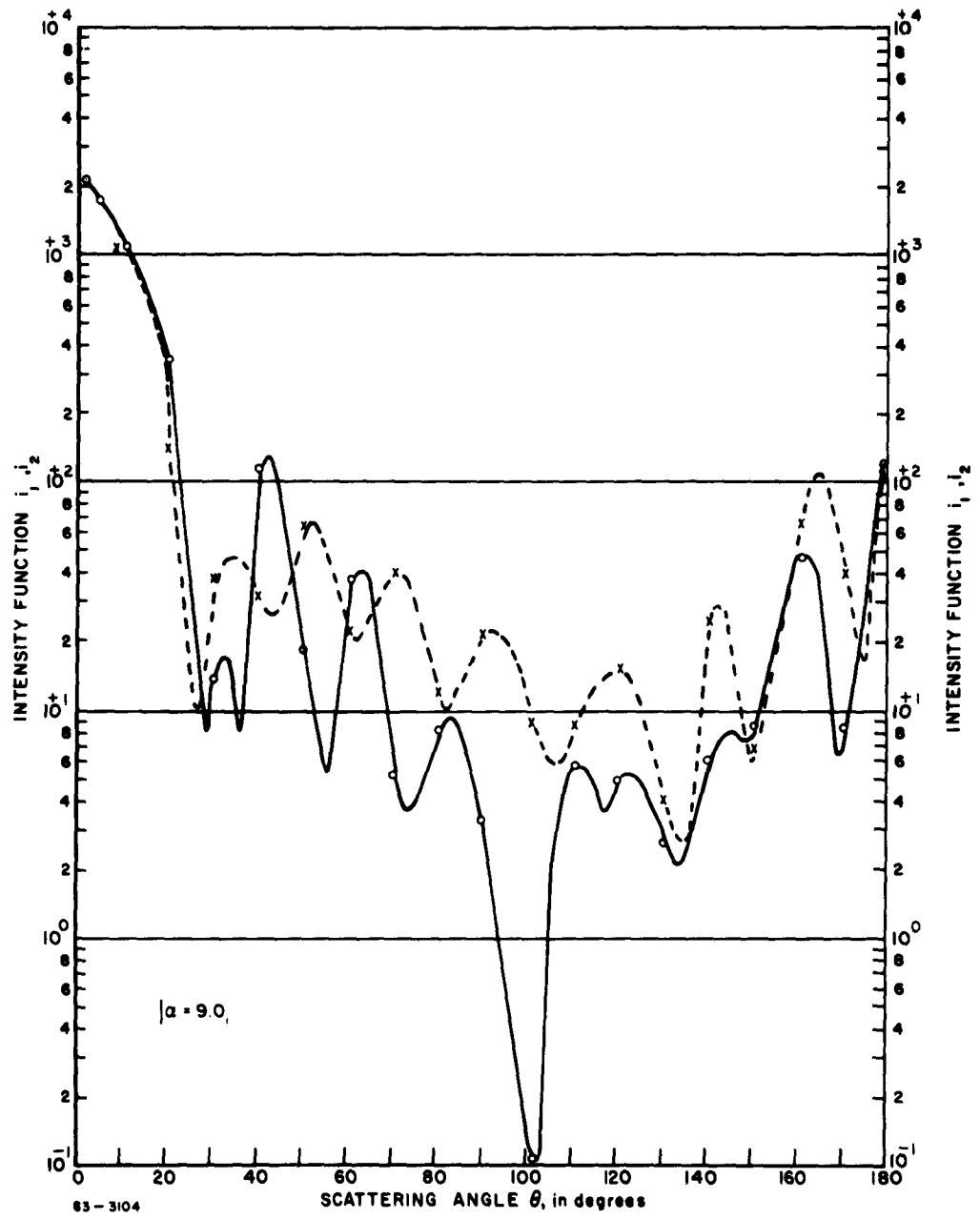


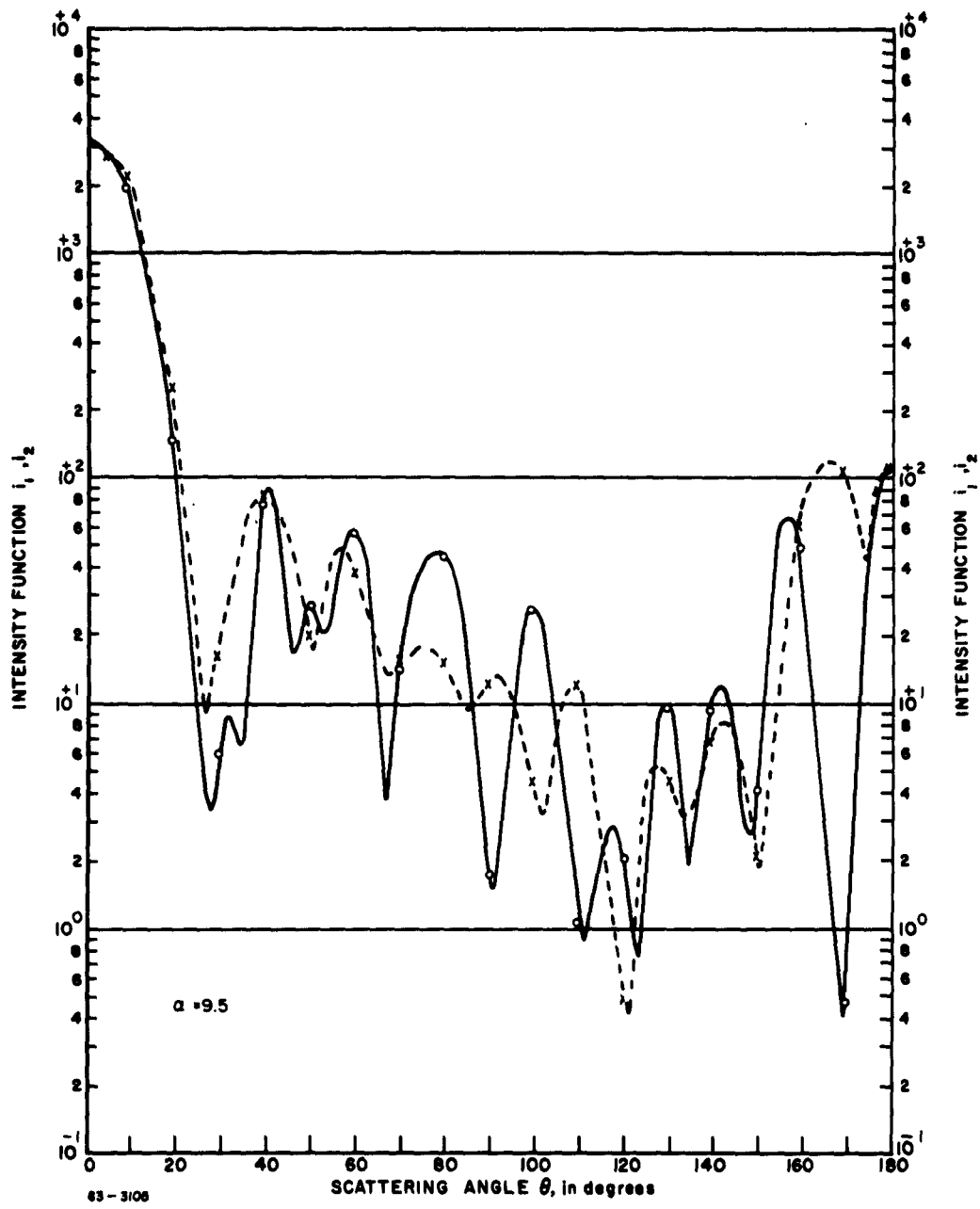


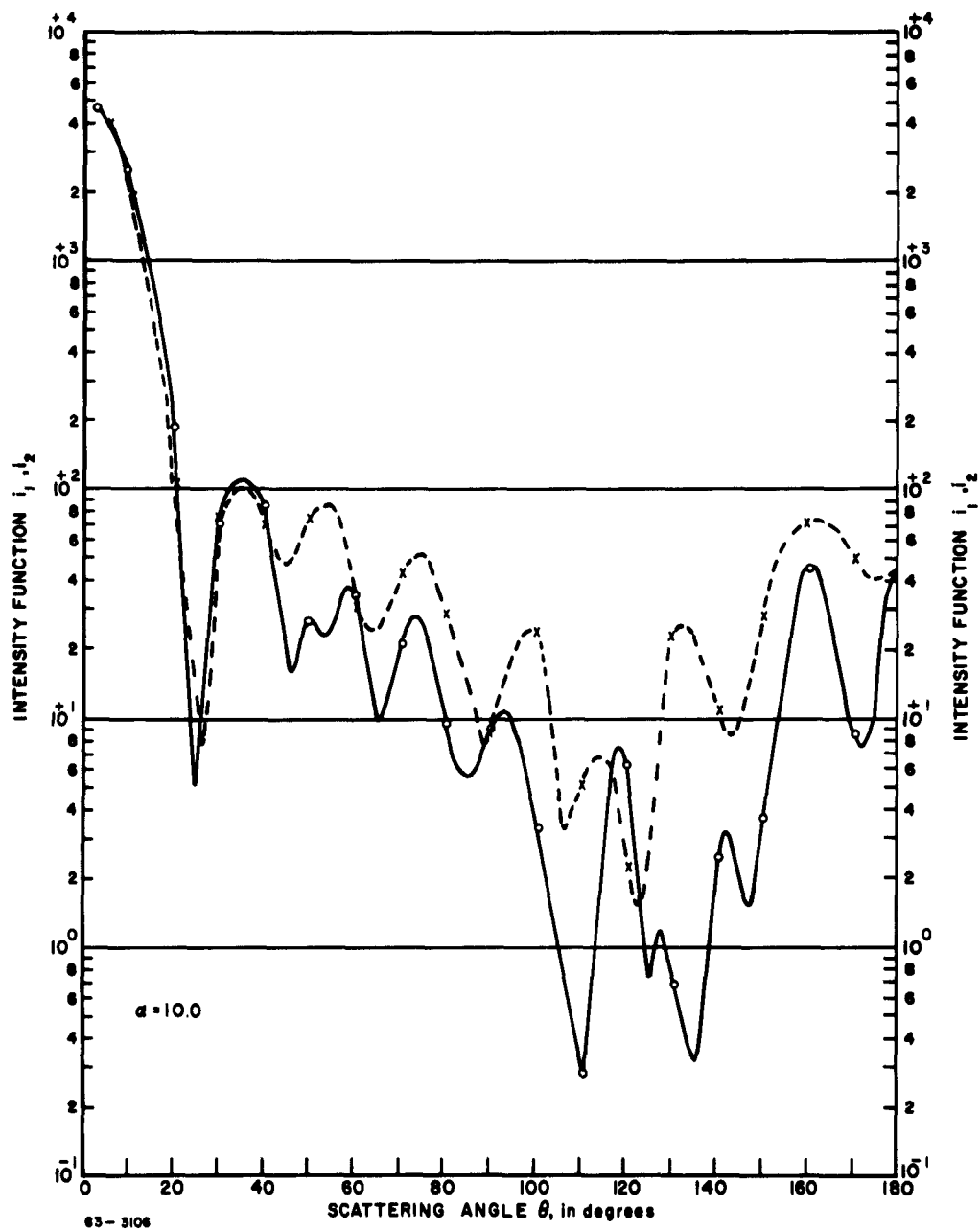












6.2 TABLE OF DARK-RING PARAMETERS FOR INTENSITY FUNCTIONS i_1
AND i_2 , $n = 1.5$ AND $\alpha = 0.5 (0.5)_{10}$

Symbols used in tables 6-1, 6-2, and 6-3 are as follows:

- α = Size parameter
- ρ = Normalized size parameter
- θ = Scattering angle in degrees ($0^\circ =$ forward)
- u = Diffraction parameter
- i_{1min} = Intensity function at minimum
- i_{1r} = Relative intensity function for particular dark ring
- D = Dark ring due to diffracted light
- T = Dark ring due to transmitted (reflected and refracted) light.

TABLE 6-1

DATA FOR INTENSITY FUNCTION i_1 AND D_1

$\alpha=0$	θ	u	i_{lmin}	$i_{lr}\{D_1\}$	$\alpha=\rho$	θ	u	i_{lmin}	$i_{lr}\{D_1\}$
2.0	123	2.30	3.6^{-3}	3.8^{-4}	26.0	7	3.33	1.5^2	1.2^{-3}
2.5	90	2.50	3.2^{-1}	1.0^{-2}	26.5	7	3.16	1.5^2	1.1^{-3}
3.0	74	2.88	1.5^{-1}	1.9^{-3}	27.0	7	3.10	6.0^2	4.3^{-3}
3.5	61	3.05	2.1^0	1.2^{-2}	27.5	7	3.18	1.5^3	1.1^{-2}
4.0	53	3.19	3.5^0	1.3^{-2}	28.0	7	3.33	4.0^3	2.1^{-2}
4.5	41	2.89	4.8^0	1.1^{-2}	28.5	7	3.48	3.0^3	1.4^{-2}
5.0	35	2.87	1.5^1	2.5^{-2}	29.0	8	3.85	1.5^3	6.5^{-3}
5.5	34	3.07	1.1^1	1.7^{-2}	29.5	8	4.05	4.0^2	1.5^{-3}
6.0	29	2.91	2.0^1	2.5^{-2}	30.0	8	4.00	1.5^2	4.0^{-4}
6.5	23	2.54	1.6^0	2.3^{-2}	30.4	7	3.67	4.0^2	1.4^{-3}
7.0	19	2.28	3.5^0	5.6^{-3}	31.0	7	3.68	6.0^2	1.9^{-3}
7.5	18	2.32	4.2^0	5.7^{-3}	31.4	7	3.62	6.0^2	2.0^{-3}
8.0	20	2.73	4.4^1	5.4^{-2}	32.0	6	3.35	3.5^2	1.2^{-3}
8.5	24	3.45	4.0^1	3.1^{-2}	32.4	6	3.30	3.0^2	1.0^{-3}
9.0	28	4.07	7.8^0	3.7^{-3}	33.0	6	3.30	8.0^2	2.7^{-3}
9.5	28	4.60	3.3^0	1.0^{-3}	33.4	6	3.40	2.5^3	7.6^{-3}
10.0	26	4.37	5.0^0	9.5^{-4}	34.0	6	3.78	5.0^3	1.3^{-3}
					34.4	7	3.92	4.0^3	1.0^{-2}
19.0	11	3.60	3.5^2	8.8^{-3}	35.0	7	4.02	9.5^2	2.0^{-3}
19.5	10	3.30	4.0^1	1.0^{-3}	35.4	7	4.07	6.0^2	1.1^{-3}
20.0	9	3.00	1.0^2	2.4^{-3}	36.0	7	4.08	5.0^1	8.7^{-4}
20.5	9	3.12	2.5^2	6.2^{-3}	36.4	6	4.05	8.0^1	1.4^{-4}
21.0	9	3.21	9.0^2	1.7^{-2}	37.0	6	3.87	1.5^2	2.4^{-4}
21.5	10	3.58	2.6^3	4.2^{-2}	37.4	6	3.73	6.0^2	1.0^{-3}
22.0	10	3.94	1.1^3	1.5^{-2}	38.0	5	3.55	9.0^2	1.4^{-3}
22.5	11	4.18	4.0^2	4.4^{-3}	38.4	5	3.50	5.0^2	8.2^{-4}
23.0	11	4.23	8.0^1	8.0^{-4}	39.0	5	3.53	7.9^2	1.3^{-3}
23.5	10	3.92	9.0^1	8.2^{-4}	39.4	5	3.57	1.5^3	2.5^{-3}
24.0	10	3.96	1.0^2	7.7^{-4}	40.0	5	3.70	5.0^3	7.5^{-3}
24.5	9	3.80	1.6^2	1.3^{-3}					
25.0	8	3.65	9.0^1	7.0^{-3}					
25.5	8	3.40	4.0^1	3.1^{-3}					

TABLE 6-2

DATA FOR INTENSITY FUNCTION i_1 , DIFFRACTION

$\alpha = \rho$	D2		D3		D4		D5		D6	
	θ	u	θ	u	θ	u	θ	u	θ	u
4.5	82	4.45								
5.0	73	4.77								
5.5	69	5.12								
6.0	63	5.34								
6.5	57	5.45	76	6.30						
7.0	49	5.28	67	6.45	80	6.88				
7.5	42	5.02	60	6.41	74	7.22				
8.0	37	4.82	50	6.04	67	7.35				
8.5	35	4.86	40	5.45	61	7.42	61	7.42	79	8.32
9.0	32/35	4.74/5.14	36	5.27	54	7.28	56	7.44	73	8.58
9.5	29/35	4.60/5.44	35	5.44	46	6.85	54	7.68	67	8.74
10.0	34	5.65	34	5.65	46	7.18	54	8.04	64	8.98

TABLE 6-3

DATA FOR INTENSITY FUNCTION i_2 , REFLECTION SYSTEM

$\alpha = \rho$	T1		T2		T3		T4		T5	
	θ	u								
2.5	138	3.33								
3.0	145	4.28								
3.5	151	5.31	105	3.63						
4.0	156	6.38	104	4.14						
4.5	157	7.25	122	5.20						
5.0	157	8.05	123	5.81	95	5.00				
5.5	161	9.22	130	6.80	101	5.62				
6.0	162	10.18	131	7.44	109	6.34	87	5.97		
6.5	164	11.22	139	8.68	114	7.07	91	6.55		
7.0	167	12.30	139	9.44	125	8.20	101	7.15		
7.5	168	13.45	141	10.25	121	8.60	103	7.70	92	7.55
8.0	171	14.85	143	11.30	130	9.85	111	8.55	90	8.02
8.5	171	15.70	149	12.60	126	10.15	116	9.38	98	8.61
9.0	168	16.20	149	13.30	133	11.48	116	9.95	101	9.20
9.5	169	17.32	149	14.10	135	12.35	124	11.15	111	10.15
10.0	173	18.80	152	15.30	135	13.00	125	11.78	113	10.80

DISTRIBUTION

<u>Addressee</u>	<u>No. of Copies</u>
A. U. (Library) Maxwell AFB, Alabama	1
AWS (AWSSS/TIPD) Scott AFB, Illinois	1
AFCRL, OAR (CRXR, Mr. John Marple) L. G. Hanscom Field Bedford, Massachusetts	1
AFCRL, OAR (CRXRA) Stop 39 (Please ship under separate L. G. Hanscom Field cover as they must be sent Bedford, Massachusetts to the Documents Unit.)	20
AFCRL, OAR (CRZH, C. N. Touart) L. G. Hanscom Field Bedford, Massachusetts	1
ESD (ESRDG) L. G. Hanscom Field Bedford, Massachusetts	1
ACIC (ACDEL-7) Second and Arsenal St. Louis 18, Missouri	1
NAFEC Library Branch, Bldg. 3 Atlantic City, New Jersey Attn: RD-702	1
ASD (ASAPRD-Dist) Wright-Patterson AFB, Ohio	1
Institute of Technology Library MCLI-LIB, Bldg. 125, Area B Wright-Patterson AFB, Ohio	1
Hq. USAF (AFCSA, Secretary) Washington 25, D. C.	1
AFOSR (SRGL) Washington 25, D. C.	1

DISTRIBUTION (Cont'd)

<u>Addressee</u>	<u>No. of Copies</u>
Hq. USAF (AFRDR) Washington 25, D. C.	1
ARL (ARA-2) Library AFL 2292, Building 450 Wright-Patterson AFB, Ohio	1
Commanding Officer U.S. Army Research & Development Laboratory Fort Monmouth, New Jersey	1
Technical Documents Center Evans Signal Labs. Belmar, New Jersey	1
Army Research Office Environmental Research Division 3045 Columbia Pike Arlington 4, Virginia	1
Office of the Chief of Research & Development Department of the Army The Pentagon Washington 25, D. C.	1
Technical Information Office European Office, Aerospace Research Shell Building, 47 Cantersteen Brussels, Belgium	1
Defence Research Member Canadian Joint Staff 2450 Massachusetts Ave., N.W. Washington 8, D. C.	2
Librarian Boulder Laboratories National Bureau of Standards Boulder, Colorado	1

DISTRIBUTION (Cont'd)

<u>Addressee</u>	<u>No. of Copies</u>
ASTIA (TIPAA) Arlington Hall Station Arlington 12, Virginia	20
Documents Expediting Project (Unit X) Library of Congress Washington 25, D. C.	1
NASA Attn: Library, Code AFET-LA Stop 85 Washington 25, D. C.	1
Library National Bureau of Standards Washington 25, D. C.	1
National Research Council 2101 Constitution Ave. Washington 25, D.C.	1
Office of Secretary (DDR&E, Tech. Library) Washington 25, D.C.	1
Superintendent of Documents Government Printing Office Washington 25, D. C.	1
Science Advisor Department of State Washington 25, D.C.	1
Director of Meteorological Research U.S. Weather Bureau Washington 25, D. C.	1
Library U.S. Weather Bureau Suitland, Maryland	1

DISTRIBUTION (Cont'd)

<u>Addressee</u>	<u>No. of Copies</u>
Director, USAF Project RAND The Rand Corporation 1700 Main Street Santa Monica, California Thru A. F. Liaison Office	1
Dr. William W. Kellogg Rand Corporation 1700 Main Street Santa Monica, California	1
Institute of Aerospace Sciences, Inc. 2 East 64th Street New York 21, New York	1
Mr. Malcolm Rigby American Meteorological Society P. O. Box 1736 Washington 13, D. C.	1
Technical Reports Librarian U. S. Naval Postgraduate School Monterey, California	1
ONR (Geophysics Code N-416) Office of Naval Research Washington 25, D. C.	1
Director U. S. Naval Research Laboratory Code 2027 Washington 25, D. C.	1
Library Geophysical Institute University of Alaska P. O. Box 938 College, Alaska	1
Professor Clarence Palmer Institute of Geophysics University of California Los Angeles 24, California	1

DISTRIBUTION (Concl'd)

<u>Addressee</u>	<u>No. of Copies</u>
Dr. Joseph Kaplan Department of Physics University of California Los Angeles, California	1
Dr. A. M. Peterson Stanford University Stanford, California	1
Dr. David Fultz Department of Meteorology University of Chicago Chicago, Illinois	1
Prof. Fred L. Whipple Harvard College Observatory 60 Garden Street Cambridge 38, Massachusetts	1
Hq. AFCRL, OAR (CRZCI, Louis Elterman) L. G. Hanscom Field Bedford, Massachusetts	10
Central Files	1
Document Control	5
Research Library	160